Humans underestimate their body mass in microgravity: evidence from reaching movements during spaceflight

Zhaoran Zhang[1]†, Yu Tian[2]†, Chunhui Wang[2], Changhua Jiang[2], Bo Wang[2], Hongqiang Yu[2], Rui Zhao[2], Kunlin Wei[1,3,4,5]*

[1] School of Psychological and Cognitive Sciences, Peking University, Beijing, China

[2] National Key Laboratory of Human Factors Engineering, China Astronaut Research and Training Center, Beijing, China

[3] Beijing Key Laboratory of Behavior and Mental Health, Beijing, China

[4] Peking-Tsinghua Center for Life Sciences, Peking University, Beijing, China

[5] National Key Laboratory of General Artificial Intelligence, Beijing, China

†Zhaoran Zhang and Yu Tian are co-first authors.

*Corresponding author: wei.kunlin@pku.edu.cn (Kunlin Wei)

Abstract

Astronauts consistently exhibit slower movements in microgravity, even during tasks requiring rapid responses. The sensorimotor mechanisms underlying this general slowing remain debated. Two competing hypotheses have been proposed: either the sensorimotor system adopts a conservative control strategy for safety and postural stability, or the system underestimates body mass due to reduced inputs from proprioceptive receptors. To resolve the debate, we studied twelve taikonauts aboard the China Space Station performing a classical hand-reaching task. Compared to their pre-flight performance and to an age-matched control group, participants showed increased movement durations and altered kinematic profiles in microgravity. Model-based analyses of motor control parameters revealed that these changes stemmed from reduced initial force generation in the feedforward control phase followed by compensatory feedback-based corrections. These findings support the body mass underestimation hypothesis while refuting the strategic slowing hypothesis. Importantly, sensory estimate of bodily property in microgravity is biased but evaded from sensorimotor adaptation, calling for an extension of existing theories of motor learning.

Introduction

Successful space exploration fundamentally depends on efficient sensorimotor control under microgravity conditions, where both movement accuracy and speed are critical (Strangman et al., 2014). A consistently observed phenomenon is that astronauts exhibit slower movements during routine activities in space stations (Kubis et al., 1977). This general movement slowing persists even in controlled experimental settings where astronauts are securely fastened without concerns for postural stability or safety. Indeed, fast movements in microgravity can be disadvantageous, potentially destabilizing posture, complicating the arrest of accelerated body segments, and increasing collision risks in confined spacecraft environments (Bock, 1998; Layne et al., 2001; Paloski et al., 1999; Reschke et al., 1998; Tafforin et al., 1989). Yet even when body stability is ensured, well-practiced goal-directed actions consistently show prolonged movement durations across various tasks, from hand pointing to visual targets (Berger et al., 1997; Bock et al., 2001, 2003; Mechtcheriakov et al., 2002) to step tracking with joysticks (Newman & Lathan, 1999; Sangals et al., 1999). This slowing manifests as reduced peak speeds in hand pointing (Mechtcheriakov et al., 2002; Sangals et al., 1999; Weber & Stelzer, 2022). Despite extensive documentation of this phenomenon, the underlying sensorimotor mechanisms remain unclear (Bock et al., 1996b; Weber et al., 2019), presenting a significant challenge for optimizing human performance in space.

Two primary hypotheses have emerged to explain the slowing of goal-directed actions in microgravity. The conservative control hypothesis suggests that the sensorimotor system adopts a generalized strategy prioritizing safety and postural stability over speed (Berger et al., 1997; Bock et al., 2010; Mechtcheriakov et al., 2002). This adaptation may arise from the novel challenges of movement control in microgravity, where even simple actions can propagate unexpected forces through body segments. The persistent application of this conservative strategy, as a generalized adaptation to the novel environment, could explain the movement

slowing in microgravity. Alternatively, the body mass underestimation hypothesis builds on observations that humans consistently underestimate the mass of handheld objects in microgravity (Ross & Reschke, 1982), suggesting that similar perceptual biases might extend to the estimation of body segment properties (Bock et al., 1996b). Such misperception would directly impact the feedforward control of movement, potentially leading to systematic under-actuation of initial movements (Elliott et al., 2010, 2017).

Both hypotheses predict reduced peak speed and acceleration in microgravity, but they diverge in their predictions about movement kinematics. First, typical reaching movement exhibits a symmetrical bell-shaped speed profile, which minimizes energy expenditure while maximizing accuracy according to optimal control principles (Todorov, 2004). The conservative control hypothesis suggests a maintained temporal symmetry as longer durations are strategically planned for optimal performance, the peak speed and acceleration are thus delayed in time (Figure 1A). In contrast, the body mass underestimation hypothesis predicts that insufficient initial force generation, resulting from a systematic sensory bias in internal models that predict movement dynamics, would lead to earlier occurrence of peak speed and acceleration (Elliott et al., 2010, 2017). Previously, the timing of these peaks has shown mixed results, with some studies reporting earlier peaks (Sangals et al., 1999), others finding delays (Fowler et al., 2008), and some showing no temporal shifts (Berger et al., 1997; Mechtcheriakov et al., 2002). Second, the hypotheses make distinct predictions about feedback-based corrections during late reaching. The conservative control hypothesis suggests that movements are optimally adapted for the microgravity environment, thus requiring no additional corrections. Instead, the mass underestimation hypothesis predicts that initial underactuation would necessitate subsequent feedback-based corrections to reach the target (Chua & Elliott, 1993; Smeets & Brenner, 1995). These corrections would manifest as additional submovements, contributing to asymmetric speed profiles (Figure 1A). Current evidence for increased feedback-based corrections in

microgravity remains inconsistent: while some studies support their presence (Sangals et al., 1999), others show conflicting results (Mechtcheriakov et al., 2002) or opposite effects (Fowler et al., 2008). If present, these corrective submovements should predict movement duration prolongation, serving as crucial evidence for the mass-underestimation account for the general slowing in microgravity.

To resolve the theoretical debate, we leveraged a unique biomechanical property of arm movements: the natural variation in effective limb mass across movement directions, known as anisotropic inertia (Mussa-Ivaldi et al., 1985). Based on a two-joint arm model (Li & Todorov, 2004), reaching movements toward targets in the frontal-medial direction involve greater effective mass compared to those in the frontal-lateral direction. Based on the motor utility theory, both the magnitude and timing of peak speed and acceleration should be systematically modulated by target direction (Shadmehr et al., 2016). Similarly, if astronauts underestimate their limb mass by approximately 30% in microgravity (Crevecoeur et al., 2014), we would expect reduced peak speed/acceleration and earlier occurrence of these peaks across all the directions. Here we examined twelve taikonauts before, during, and after their 3- or 6-month missions on the China Space Station (CSS) and compared their performance to age-matched ground controls. Participants performed rapid reaching movements to targets specifically chosen to engage different effective masses. Our approach allows us to dissociate the effects of mass underestimation from strategic control by examining how movement kinematics vary with direction-dependent effective mass.

Results

We compared the performance of 12 taikonauts to that of age-matched ground controls across multiple test sessions (Figure 6B and Table S1). Participants performed rapid reaching movements toward one of three targets, presented in pseudorandom order to minimize movement automation and ensure active planning for each reach. The three target directions (45°, 90°, and 135°) were chosen to vary the effective mass of the moving limb, as verified through biomechanical simulations based on the two-joint arm model (Li & Todorov, 2004; Figure 1B). Our model simulations not only demonstrated the direction-dependent variation in limb mass but also predicted how actual and misperceived limb mass would affect reaching kinematics (Figure 1C-H). These predictions were derived by combining the movement utility framework for estimating planned movement duration (Shadmehr et al., 2016; Figure S1A-B) with a forward optimal controller for simulating reaching trajectories (Todorov, 2005; Figure S1C-D). Notably, the model predicted that underestimating limb mass would lead to reduced and earlier peak speed/acceleration across directions (Figure 1C-H).

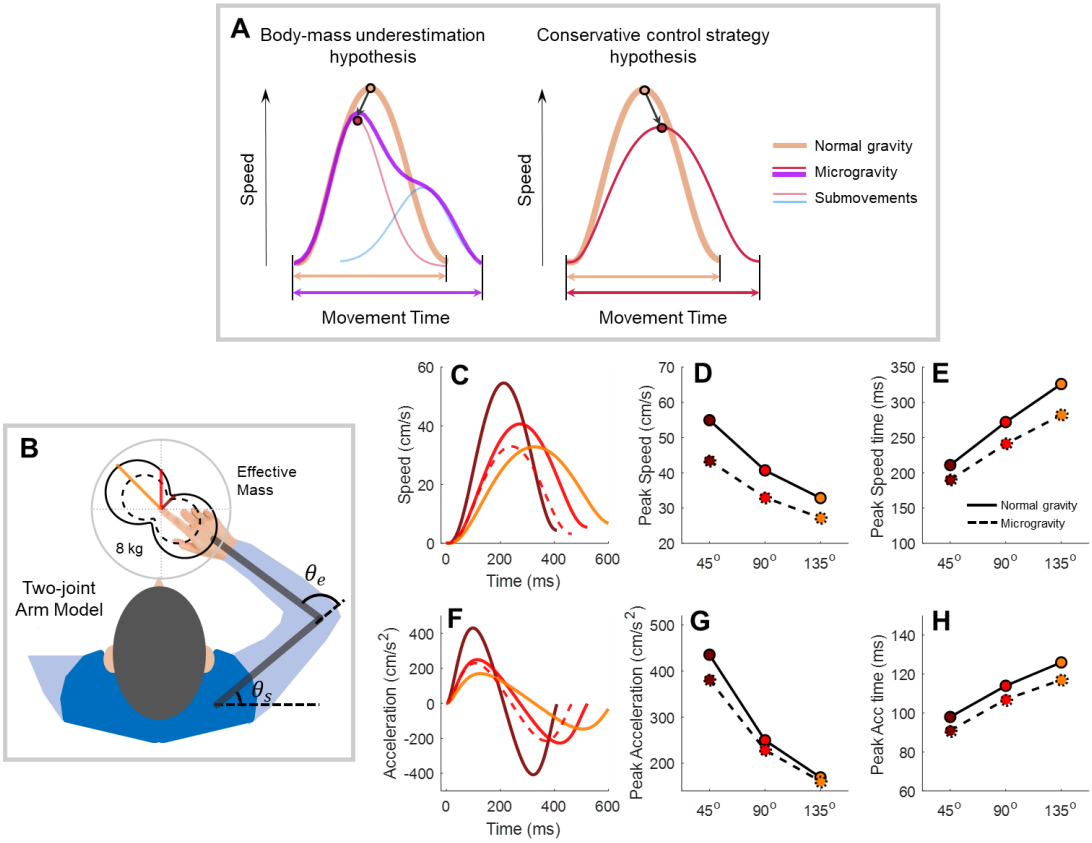

Figure 1. Model simulations revealing characteristic kinematic features of reaching movements. A) Speed profile predictions under two competing hypotheses. Under normal gravity, hand speed follows a typical profile (bold apricot lines). According to the body mass underestimation hypothesis (left panel), initial underactuation produces a lower, earlier peak speed (light red), necessitating a corrective submovement (light blue) that results in an asymmetric, prolonged profile (purple). The conservative strategy hypothesis (right panel) predicts symmetric slowing with delayed peak speed (red). **B)** Two-joint arm model and its simulated effective mass. The spatial distribution of effective mass is shown by black curves (solid: normal gravity; dashed: 30% mass underestimation in microgravity). Colored lines indicate effective mass values for our three experimental target directions (45°, 90°, 135°). **C & F)** Representative speed and acceleration profiles simulated using effective masses from B. Profiles shown for normal (solid) and underestimated (dashed) body mass in the 90° direction demonstrate reduced, earlier peaks with mass underestimation. **D-E & G-H)** Simulated kinematic parameters across movement directions under normal (solid) and underestimated (dashed) mass conditions. Mass underestimation consistently leads to reduced amplitude and

earlier timing of speed/acceleration peaks across all directions. Model simulation details provided in Supplementary Note 1.

Movement Accuracy and Reaction Time Remain Intact in Microgravity.

All participants successfully completed the task. Invalid trials, comprising early initiation (RT < 150 ms), late initiation (RT > 400 ms), or measurement failures, accounted for only 1.87% of trials in the experimental group and 0.70% in the control group. The percentage of invalid trials remained stable across the pre- in and post-flight phases (Friedman's tests, all $p > 0.1$).

Reaching accuracy remained high despite the stringent speed requirement of completing movements within 650 ms after target appearance (Figure S2). Analysis of endpoint error using a 3 (target direction) × 3 (phase) repeated-measures ANOVA revealed no significant differences across phases for either group. While the experimental group showed slightly better accuracy for the 45° target, this difference was minimal (0.04 cm over a 12 cm reach distance).

In half of the trials, a beep accompanied target appearance to promote faster reactions, allowing us to examine speed-accuracy trade-offs during action planning (Sutter et al., 2021). The beep effectively reduced median reaction times by approximately 38 ms (242 ± 49 ms vs. 281 ± 50 ms; Figure 2A; see control group data in Figure S3A). To evaluate microgravity effects, we pooled data from both beep conditions and conducted a 3 (direction) × 3 (phase) repeated-measures ANOVA. The experimental group showed significant main effects of direction ($F(2,22) = 25.260$, $p < 0.001$, partial $\eta^2 = 0.697$) and phase ($F(2,22) = 5.820$, $p = 0.014$, partial $\eta^2 = 0.346$), without interaction ($F(4,44) = 2.246$, $p = 0.111$). Post-hoc analyses revealed slower reaction times for the 45° direction compared to both 90° ($p < 0.001$, d = 0.293) and 135° ($p = 0.003$, d = 0.284). Notably, reactions were faster during the in-flight phase compared to pre-flight ($p = 0.037$, d = 0.333), with no significant difference between in-flight and post-flight

phases (p = 0.127). Similar effects were observed in the control group (Figure S3A), suggesting that the reduced reaction times likely reflect practice effects rather than microgravity influence. Thus, participants maintained, and even improved, their ability to rapidly initiate movements in microgravity with reaching accuracy.

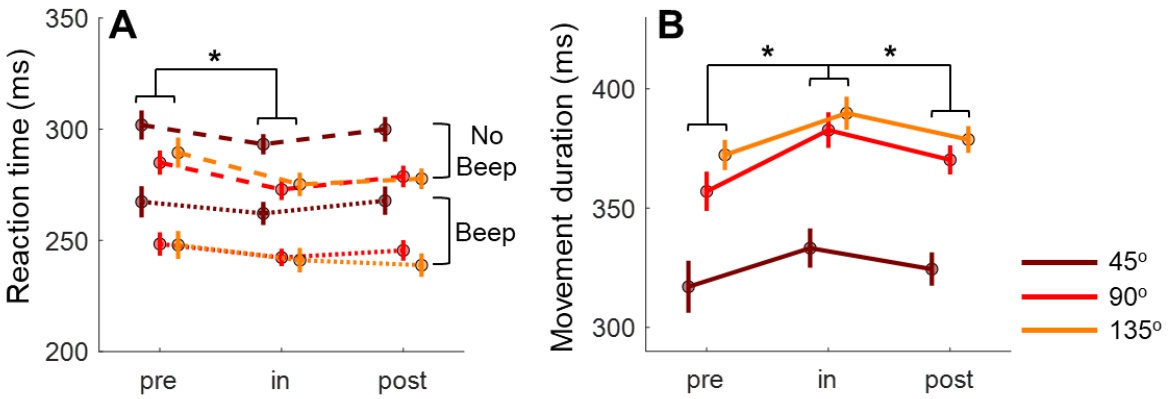

Figure 2. Reaction time and movement duration in the experimental group. A) Median reaction times plotted by experimental phase (x-axis) and target direction (different colors). Dashed lines and dot lines represent the "beep" and "no beep" conditions. **B)** Average movement durations shown in the same format. Data are combined across beep conditions due to no significant differences between them. In both panels, error bars denote standard error across participants. Asterisks indicate significance levels for post-hoc phase comparisons (*p < 0.05, **p < 0.01, ***p < 0.001).

Microgravity leads to slower movement.

Although showing no decrement in movement accuracy or RT, the taikonauts exhibited prolonged movement durations (MD) during the in-flight phase compared to both pre- and post-flight phases (Figure 2B). A two-way repeated-measures ANOVA reveals significant main effects of direction ($F(2,22) = 62.555$, $p < 0.001$, partial $\eta^2 = 0.850$) and phase ($F(2,22) = 6.761$,

p = 0.015, partial η^2 = 0.381), with no significant interaction ($F(4,44) = 1.413$, p = 0.263). Post-hoc comparisons showed that MD was significantly prolonged during the in-flight phase (vs. pre-flight: p = 0.014, d = 0.333; vs. post-flight: p = 0.013, d = 0.181). MD was also significantly greater for the 90° and 135° directions—those associated with larger effective mass—compared to the 45° direction (all $p < 0.001$ in pairwise comparisons). In contrast, the control group showed a similar directional effect but, importantly, did not show a phase effect (Figure S3B), suggesting that movement slowing is specific to spaceflight.

Microgravity leads to reduced peak acceleration/speed and advanced timing of these peaks.

The initial movement exhibited signs of underactuation during spaceflight, consistent with the body mass underestimation hypothesis. Peak acceleration and peak speed, established measures of feedforward control (Elliott et al., 2010, 2017), both showed significant decreases during the in-flight phase (Figure 3). For peak acceleration, there were significant main effects of phase ($F(2,22) = 6.401$, p = 0.015, partial η^2 = 0.368) and direction ($F(2,22) = 75.516$, $p < 0.001$, partial η^2 = 0.873), along with an interaction effect ($F(4,44) = 4.548$, p = 0.016, partial η^2 = 0.293). Consistent with model simulations, the 45° direction, associated with a lower effective mass, showed significantly higher peak acceleration than the other two directions (Figure 3A; all $p < 0.001$ in pairwise comparisons). Peak acceleration decreased significantly during spaceflight across all three directions (simple main effects: 45°, p = 0.020, η^2 = 0.543; 90°, p = 0.004, η^2 = 0.673; 135°, p = 0.005, η^2 = 0.657). Planned contrasts further indicated lower peak acceleration in the in-flight phase compared to pre-flight (45°, p = 0.006, η^2 = 0.516; 90°, p = 0.008, η^2 = 0.485; 135°, p = 0.003, η^2 = 0.560), with marginal recovery in the post-flight phase for two directions (45°, p = 0.071, η^2 = 0.267; 90°, p = 0.062, η^2 = 0.282) and significant recovery for one direction (135°, p = 0.029, η^2 = 0.363).. In contrast, the control group displayed only the direction effect (Figure S3C-D), confirming that the underactuation was specific to microgravity.

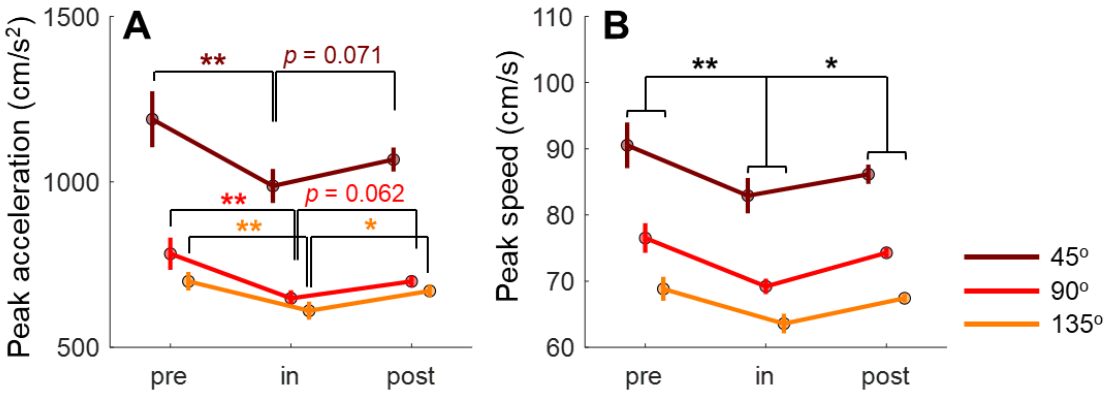

Figure 3. Magnitude changes of peak acceleration and speed during spaceflight. A) Peak acceleration across experimental phases and movement directions, showing systematic decreases during the in-flight phase. **B)** Peak speed data presented in the same format, demonstrating parallel changes to peak acceleration. Error bars indicate standard error across participants. Statistical significance levels are shown for both overall phase comparisons (black asterisks) and planned contrasts within each direction (colored asterisks): *$p < 0.05$, **$p < 0.01$, ***$p < 0.001$.

Peak speed showed parallel changes during spaceflight (Figure 3B). Analysis revealed significant main effects of phase ($F(2,22) = 7.043$, $p = 0.009$, partial $\eta^2 = 0.390$) and direction ($F(2,22) = 114.420$, $p < 0.001$, partial $\eta^2 = 0.912$), without interaction ($F(4,44) = 1.929$, $p = 0.161$). Peak speed was significantly reduced during the in-flight phase compared to both pre-flight ($p = 0.004$, d = 0.331) and post-flight phases ($p = 0.046$, d = 0.199), with evidence of recovery post-flight (pre- vs. post-flight: $p = 0.483$, d = 0.132). Target direction systematically modulated peak speed (all pairwise comparisons, $p < 0.001$), with the 45° direction showing highest speeds and 135° lowest—matching predictions based on the movement utility theory. The control group showed only direction effects without phase-related changes (Figure S3D), confirming the specificity of these changes to microgravity exposure.

The critical test for the competing hypotheses of movement slowing lies in whether peak acceleration and peak speed occur earlier or later in microgravity. The body mass underestimation hypothesis predicts earlier timing, whereas the conservative control strategy hypothesis predicts delayed timing. We observed an overall timing advance of these two measures. For peak acceleration time in the experimental group (Figure 4A), two-way repeated-measures ANOVAs revealed significant main effects of phase ($F(2,22) = 5.189$, $p = 0.024$, partial $\eta^2 = 0.321$) and direction ($F(2,22) = 30.375$, $p < 0.001$, partial $\eta^2 = 0.734$), along with an interaction effect ($F(4,44) = 4.503$, $p = 0.013$, partial $\eta^2 = 0.290$). In line with predictions, peak acceleration appeared significantly earlier in the 45° direction than other directions (45° vs. 90°, $p < 0.001$, d = 0.304; 45° vs. 135°, $p < 0.001$, d = 0.271). The phase effect emerged only for directions with higher effective mass (simple main effects, 90°: $F(2,10) = 6.660$, $p = 0.015$, $\eta^2 = 0.571$; 135°: $F(2,10) = 8.411$, $p = 0.007$, $\eta^2 = 0.627$). Planned contrasts confirmed earlier peak acceleration during spaceflight compared to post-flight (90°, $p = 0.005$, $\eta^2 = 0.530$; 135°, $p = 0.004$, $\eta^2 = 0.537$), with marginal differences versus pre-flight (135°, $p = 0.065$). The control group showed only directional effects without phase effect (Figure S3E).

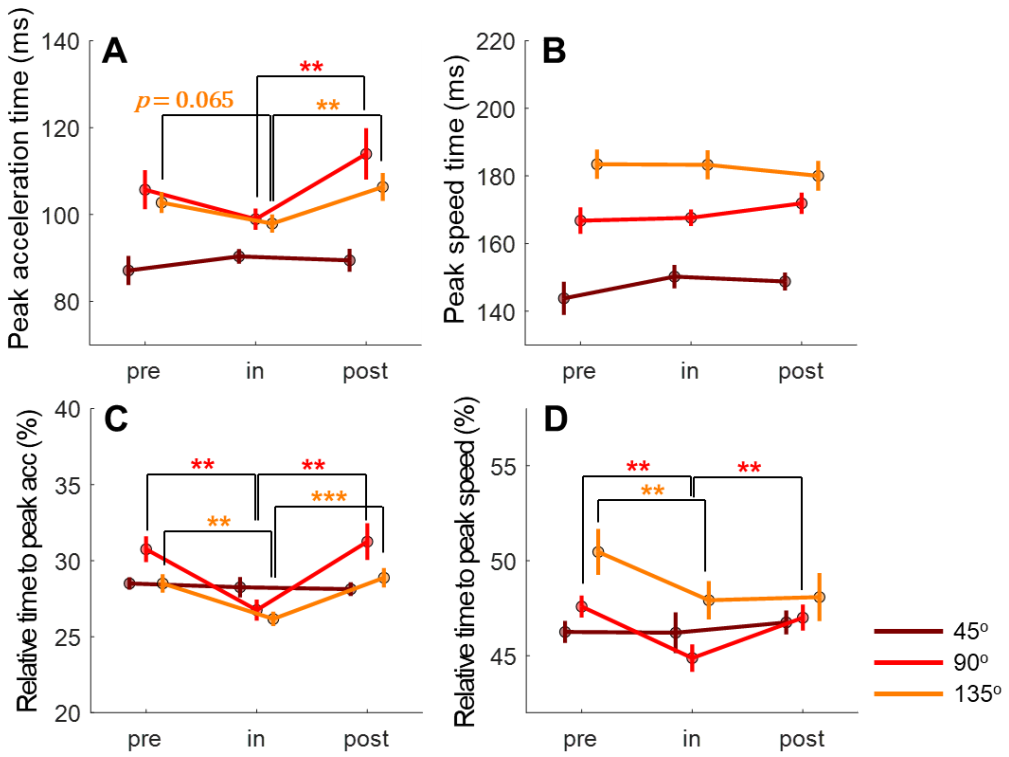

Figure 4. Temporal analysis of peak acceleration and peak speed during spaceflight. A-B) Time to peak acceleration and peak speed across experimental phases and movement directions. **C-D)** Relative timing analysis showing these same peaks as a percentage of total movement duration, revealing more pronounced microgravity effects than absolute timing measures. Error bars indicate standard error across participants. Asterisks denote significance levels for planned phase comparisons (*p < 0.05, **p < 0.01, ***p < 0.001). Note the systematic modulation of timing by phase, particularly for high effective mass conditions.

Given that overall movement duration is prolonged in microgravity, a more direct way to assess the symmetry of the speed profile is to compute the relative timing of speed/acceleration peaks as a percentage of MD. Indeed, the relative timing of peak acceleration showed the same reduction in microgravity with a more pronounced effect than absolute timing (Figure 4C). A two-way repeated-measures ANOVA revealed significant main effects of phase ($F(2,22) = 15.414$, $p < 0.001$, partial $\eta^2 = 0.584$) and interaction ($F(2,22) = 7.223$, $p = 0.002$, partial η^2 =

0.396), while the main effect of direction was marginally significant ($F(2,22) = 3.374$, $p = 0.053$, partial $\eta^2 = 0.235$). Phase effects were significant for directions with higher effective mass (simple main effects: 90°, $F(2,10) = 13.327$, $p = 0.002$, $\eta^2 = 0.727$; 135°, $F(2,10) = 24.574$, $p < 0.001$, $\eta^2 = 0.831$) but not for 45° ($F(2,10) = 0.609$, $p = 0.563$). Planned contrasts confirmed significantly earlier timing during spaceflight compared to both pre- and post-flight phases (all $p < 0.002$ for 90° and 135° directions). None of these effects appeared in the control group (Figure S3G).

Peak speed also showed a timing advance, but only for relative timing. For absolute timing (Figure 4B), a two-way repeated-measures ANOVA revealed a significant main effect of direction ($F(2,22) = 57.428$, $p < 0.001$, partial $\eta^2 = 0.839$) and a marginal interaction ($F(4,44) = 2.233$, $p = 0.095$, partial $\eta^2 = 0.169$), without a phase effect ($F(2,22) = 0.093$, $p = 0.864$). In contrast, relative timing analysis (Figure 4D) showed significant effects of phase ($F(2,22) = 8.941$, $p = 0.004$, partial $\eta^2 = 0.448$), direction ($F(2,22) = 4.991$, $p = 0.030$, partial $\eta^2 = 0.312$), and their interaction ($F(4,44) = 4.755$, $p = 0.015$, partial $\eta^2 = 0.302$). The phase effect appeared only for directions with higher effective mass (90°: $F(2,10) = 17.278$, $p = 0.001$, $\eta^2 = 0.776$; 135°: $F(2,10) = 6.189$, $p = 0.018$, $\eta^2 = 0.553$). Planned contrasts revealed significantly earlier relative timing during spaceflight versus pre-flight for both 90° ($p < 0.001$, $\eta^2 = 0.770$) and 135° ($p = 0.007$, $\eta^2 = 0.496$) directions, with significant post-flight recovery in 90° ($p = 0.003$, $\eta^2 = 0.575$). The control group showed only directional effects (Figure S3F & 2H). Thus, after accounting for the prolongation of movement duration, we observed a temporal advance of peak acceleration and speed during spaceflight.

Movement slowing is associated with corrective submovements.

The feedforward component of movement, captured by our model simulations, accounts for only the initial phase of reaching. With peak acceleration and speed occurring at approximately 80

ms and 150 ms after movement onset, and total movement duration spanning 300-400 ms, participants had ample opportunity for feedback-based corrections (Dimitriou et al., 2013). These corrections, if present, would manifest as secondary submovements (Meyer et al., 1988). While optimal reaching movements typically show symmetrical speed profiles (Flash & Hogan, 1985), the presence of corrective submovements creates characteristic left-skewed speed profiles (Elliott et al., 2010; Meyer et al., 1988; Woodworth, 1899). To identify such corrections, we employed an established decomposition method (Rohrer & Hogan, 2006) to detect trials containing both primary and secondary submovements (two-peak trials; Figure 5A).

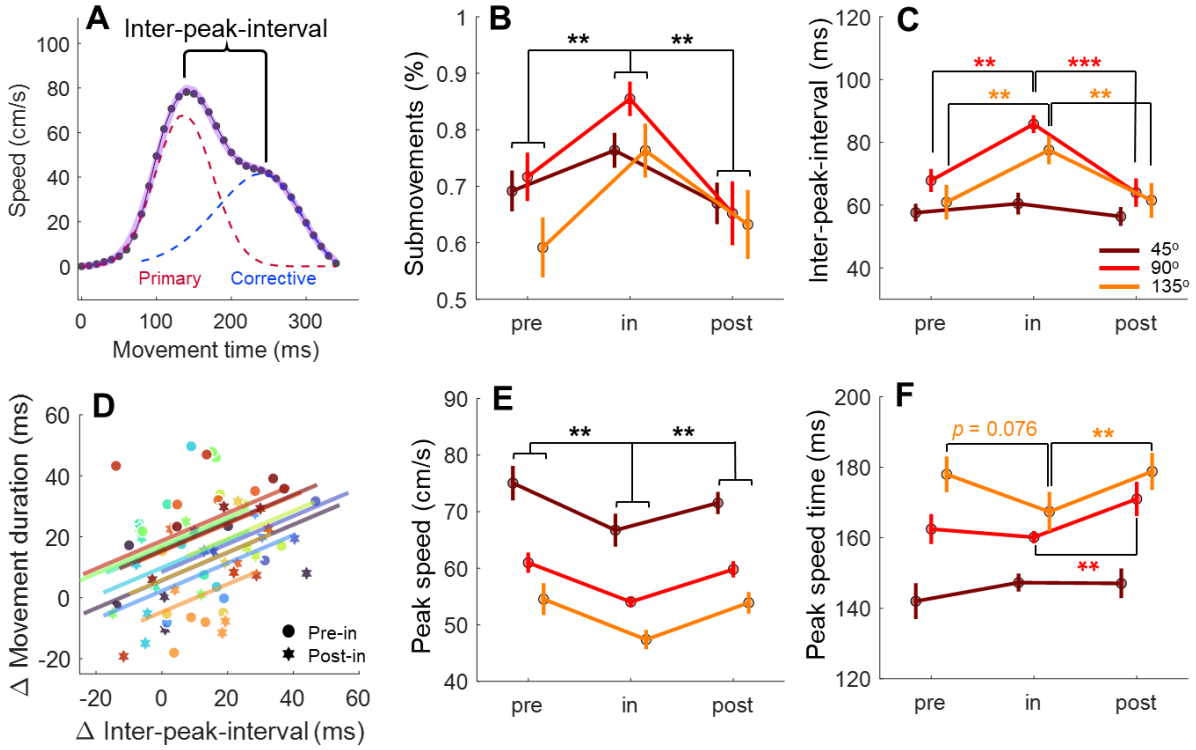

Figure 5. Submovements analysis revealed changes in corrective movements during spaceflight. A) Decomposition of a representative two-peak speed profile, illustrating primary and corrective submovements separated by the inter-peak interval (IPI). **B)** Proportion of movements showing corrective submovements across phases and directions. **C)** Magnitude of feedback corrections quantified by IPI, showing direction-dependent increases in microgravity.

D) Linear relationship between feedback correction changes (ΔIPI) and movement slowing (ΔMD). Each participant (shown in different colors) contributed multiple data points from different phases and directions. **E-F)** Primary submovement characteristics: peak speed amplitude and timing. Error bars denote standard error across participants; asterisks indicate significance (*$p < 0.05$, **$p < 0.01$, ***$p < 0.001$).

Analysis revealed a striking increase in corrective movements during spaceflight. The percentage of trials showing two distinct submovements increased significantly during the in-flight phase (Figure 5B), evidenced by a main effect of phase ($F(2,22) = 13.969$, $p < 0.001$, partial $\eta^2 = 0.559$) and a marginal phase-by-direction interaction ($F(2,22) = 2.642$, $p = 0.054$, partial $\eta^2 = 0.194$). This effect was specific to microgravity exposure, as the control group showed no significant changes across phases (all $p > 0.05$; Figure S4A). Notably, the increase in corrective movements was most pronounced for directions with higher effective mass (simple main effects: 90°, $F(2,10) = 11.426$, $p = 0.003$, $\eta^2 = 0.696$; 135°, $F(2,10) = 7.292$, $p = 0.011$, $\eta^2 = 0.593$).

To understand how feedback corrections contribute to movement slowing, we analyzed the inter-peak interval (IPI) between primary and corrective submovements, an established measure of feedback-based control (Craik, 1947; Meyer et al., 1988, 2018). The taikonauts showed markedly longer IPIs during spaceflight (Figure 5C), with a two-way ANOVA revealing significant effects of phase ($F(2,22) = 11.150$, $p = 0.001$, partial $\eta^2 = 0.503$), direction ($F(2,22) = 4.721$, $p = 0.026$, partial $\eta^2 = 0.300$), and their interaction ($F(2,22) = 6.559$, $p = 0.002$, partial $\eta^2 = 0.374$). Critically, IPI increases were confined to directions with greater effective mass (90°, $F(2,10) = 11.573$, $p = 0.002$, $\eta^2 = 0.698$; 135°, $F(2,10) = 13.371$, $p = 0.001$, $\eta^2 = 0.728$). The control group exhibited only directional effects ($F(2,22) = 19.277$, $p < 0.001$, partial $\eta^2 = 0.637$; Figure S4B) without phase-related changes (all $p > 0.13$).

To establish whether these enlarged corrective movements explain the overall movement slowing, we examined how changes in IPI (ΔIPI) predict changes in movement duration (ΔMD) during spaceflight (Figure 5D). A Linear Mixed Model analysis incorporating ΔIPI, phase transition (pre-to-in and post-to-in), and direction revealed that ΔIPI significantly predicted ΔMD (β = 0.458 [0.144, 0.771], t(67) = 2.915, p = 0.005, partial-R^2 = 0.103). Phase transition also showed significance (β = -0.01 [-0.017, -0.001], t(67) = -2.696, p = 0.009, partial-R^2 = 0.086), with stronger effects for pre-to-in versus post-to-in transitions, indicating incomplete recovery post-flight. Movement direction showed no significant effect (all p > 0.42), suggesting that the relationship between corrective movements and duration slowing generalizes across reaching directions.

The analysis of primary submovements revealed even stronger evidence for feedforward control changes in microgravity. By focusing on just the primary submovement in two-peak trials, we found more pronounced effects than when analyzing the overall movement (comparing Figure 5E to Figure S4C). The primary submovement showed a robust reduction in peak speed during spaceflight (main effect of phase: F(2,22) = 10.363, p = 0.001, partial η^2 = 0.485) that was consistent across directions (interaction: F(4,44) = 0.382, p = 0.711; Figure 5E). More tellingly, while the overall movement showed timing changes only in relative measures, the primary submovement exhibited earlier peak speed timing in absolute terms (phase-by-direction interaction: F(2,22) = 4.264, p = 0.012, partial η^2 = 0.279). This temporal advance was most evident in directions with higher effective mass (planned contrasts vs. post-flight: 135°: p = 0.008, η^2 = 0.615; 90°: p = 0.076, η^2 = 0.403) but absent in the 45° direction (p = 0.188, η^2 = 0.284). The selective nature of the primary submovement in both magnitude and timing (comparing Figure 4B and Figure 5F) provides compelling evidence for mass-dependent changes in feedforward control. The control group showed only the expected directional

variations ($F(2,22) = 46.259$, $p < 0.001$, partial $\eta^2 = 0.808$; Figure S4D) without any phase effects (all $p > 0.13$), confirming these changes as specific to microgravity exposure.

Speed-accuracy trade-offs remain intact during spaceflight.

The speed-accuracy trade-off, a fundamental indicator of motor control efficiency, remained largely intact during spaceflight. We evaluated this trade-off using two complementary approaches. First, following the traditional Fitts' framework (Plamondon & Alimi, 1997), we examined the relationship between movement duration and endpoint dispersion, which was not negatively affected by microgravity (Figure S5). Second, we analyzed the trade-off between reaction time and initial movement variance (Figure S6), which reflects the quality of movement planning (Sutter et al., 2021). This relationship persisted across all phases in both groups. Thus, while microgravity altered movement execution through mass underestimation, it did not fundamentally disrupt the sensorimotor system's capacity to regulate the speed-accuracy trade-off.

Discussion

Long-term exposure to microgravity presents a unique environment that cannot be replicated on Earth, offering invaluable insights into human sensorimotor adaptation. Understanding how microgravity affects motor performance is crucial both for ensuring successful space exploration and for advancing our fundamental knowledge of motor control principles. Our study elucidates the mechanisms underlying one of the most distinctive motor signatures in microgravity: the slowing of goal-directed actions during spaceflight. While taikonauts maintained reaching accuracy and rapid reaction times, their movements exhibited systematic changes in microgravity characterized by reduced peak speed and acceleration, along with advanced

timing of these peaks. These kinematic alterations persisted across repetitive trials within a session and also persisted across multiple sessions during spaceflight (Figure S7), contradicting the hypothesis that astronauts adopt a conservative control strategy to maintain stability. Instead, they align precisely with our hypothesis that individuals underestimate limb effective mass, leading to underactuated initial movements. These changes followed model predictions across movement directions with varying effective masses due to limb biomechanics, confirming that the representation of body mass indeed affects movement control during spaceflight. Beyond the initial underactuation caused by altered feedforward control, we observed increased feedback-based corrective submovements that predicted movement duration prolongation in spaceflight. These effects were specific to microgravity exposure, occurring only during spaceflight with marked recovery post-flight, while ground controls showed no comparable changes. Notably, the taikonauts' fundamental motor control capabilities remained largely intact, as evidenced by preserved movement accuracy, reaction time, and speed-accuracy trade-offs.

The underactuation observed in initial movements under microgravity extends findings from parabolic flight studies (Crevecoeur et al., 2014; Papaxanthis et al., 2005). When individuals performed reaching movements with handheld weights during parabolic flight-induced gravity alterations, their reaching trajectories and grip forces showed systematic changes suggesting mass misperception (Bock, 1998; Bock et al., 1996a, 1996b; Crevecoeur et al., 2014; Papaxanthis et al., 2005). In zero-gravity conditions, goal-directed arm movements were slower (Papaxanthis et al., 2005), and grip-load force coordination was altered (Crevecoeur et al., 2010, 2014), consistent with mass underestimation. Conversely, hypergravity (1.8g) induced increased peak acceleration and speed in reaching movements, along with elevated grip force during object manipulation, suggesting mass overestimation (Bock, 1998; Bock et al., 1992, 1996a, 1996b). Notably, modified grip-load force coordination reflects changes in feedforward control (Flanagan & Wing, 1997; Johansson & Edin, 1993), indicating that mass misestimation

influences action planning. However, while parabolic flight studies capture only transient adaptations to rapid gravity transitions, our study targets general slowing during spaceflight and reveals the enduring effects of sustained microgravity exposure.

Our results strongly challenge the conservative control strategy hypothesis, which posits that movement slowing reflects a generalized adaptation to address stability or safety concerns during spaceflight (Bock, 1998). Contrary to this hypothesis, taikonauts demonstrated faster reaction times during spaceflight—incompatible with a generalized slowing strategy. More critically, if the sensorimotor system adopted a conservative strategy with pre-planned longer movement durations, the speed profile should maintain symmetry with delayed peak acceleration and speed. Instead, we observed left-skewed speed profiles with earlier peak occurrence, directly contradicting the predictions of strategic slowing. This temporal change was more pronounced if primary submovement is isolated to pinpoint the feedforward control of the reaching since the overall speed profile is affected by the later feedback-based corrections. Previous studies reported inconsistent findings regarding speed profile symmetry, including advanced (Sangals et al., 1999), delayed (Fowler et al., 2008), or unchanged (Berger et al., 1997; Mechtcheriakov et al., 2002) peak speed timing during spaceflight. These discrepancies likely reflect methodological differences, including task variations and technical limitations. For example, two studies used joystick-based pointing tasks without involving limb movement (Fowler et al., 2008; Sangals et al., 1999), which arguably makes them less suitable for examining mass underestimation effects. Mechtcheriakov and colleagues used an outstretched arm task, but their limited sampling rate of 25 Hz may have hindered precise quantification of peak speed, preventing submovement analysis. Additionally, our larger sample size (n = 12) may have enhanced detection of microgravity effects compared to previous studies with typically 3-7 participants (Berger et al., 1997; Bock et al., 2001, 2003, 2010; Fowler et al., 2008;

Mechtcheriakov et al., 2002; Papaxanthis et al., 1998; Weber & Stelzer, 2022) or single-participant designs (Heuer et al., 2003; Manzey et al., 1998; Sangals et al., 1999).

The underestimation of body mass in microgravity likely arises through two complementary mechanisms: degraded proprioceptive feedback and misinterpretation of weight-related cues. Microgravity impairs proprioception by reducing both muscle spindle sensitivity (Lackner & DiZio, 1992) and joint receptor responsiveness (Proske & Weber, 2023)—inputs that are crucial for weight perception (Proske & Gandevia, 2012). Furthermore, the sensorimotor system may interpret weight unloading as reduced body mass rather than environmental change (Bock et al., 1996b). Recent studies demonstrate that the sensorimotor system probabilistically infers body-versus-environment causality based on available sensory cues (Berniker & Kording, 2008; Fercho & Baugh, 2014; Kluzik et al., 2008; Kong et al., 2017; Wilke et al., 2013). In normal gravity, consistent mass-weight relationships lead to heavy reliance on weight-related cues for mass estimation (Bock, 1998; Bock et al., 1996b; Sangals et al., 1999). In microgravity, however, reduced weight cues become misleading and may systematically bias mass perception, affecting feedforward control of movement.

The persistence of deviant feedforward control and the subsequent within-movement corrections appears intriguing from the theories of human motor learning. Humans demonstrate remarkable ability to adapt to environmental changes in terrestrial studies. For experimentally-applied visual or force perturbations, individuals can recalibrate their sensorimotor control and restore baseline performance within minutes (Krakauer et al., 2019), a process often theorized as forming internal models of the new environment (Kawato, 1999; Wolpert et al., 1995). Relatedly, even when the body mass is perturbed by attaching a weight on the forearm, individuals can fully adapt their reaching movements within tens of trials (Wang & Sainburg, 2004). Our in-flight sessions were scheduled at least three weeks post-launch—even well beyond the 2-3 weeks window typically considered critical for sensorimotor adaptation in

spaceflight (Kanas & Manzey, 2008), but the participants still exhibited un-adapted feedforward control and internal model.

We believe this contrast stems from distinct natures of perturbation effects in microgravity when compared to in terrestrial environments. Previous studies on sensorimotor adaptation simulated environmental changes by imposing a perturbation to alter the relationship between motor commands and sensory consequences of motor commands. For reaching adaptation here, visuomotor perturbations changes the spatial mapping between hand motion and its visual representation's motion (Krakauer et al., 2000; Wolpert et al., 2011); force perturbations change the dynamic mapping between actual force outputs and hand motion (Lackner & Dizio, 1994; Shadmehr & Mussa-Ivaldi, 1994). These mapping changes, though novel, are consistent thus the sensorimotor system is capable of approximating them and adapting accordingly. Theories of sensorimotor adaptation conceptualize the formation of the new mapping as acquiring internal models, which links motor command and efference copy to sensory consequences of motor commands (Flanagan & Wing, 1997; Kurtzer et al., 2008; Wolpert et al., 1998; Wolpert & Miall, 1996). However, the novel environment of microgravity alters the sensory estimate of motor apparatus (i.e., the body mass here), not merely the sensorimotor mapping. In normal gravity, weight-related sensory cues—mostly proprioceptive feedback—accurately represent body mass. In microgravity, however, these weight-related cues are substantially reduced due to the absence of gravitational pull, providing persistently biased information about body mass. Body mass is a parametric input to the internal models, thus its bias would affect motor actions even when the internal models are well adapted. Hence, the unique environment of microgravity reveals a fundamental constraint of the sensorimotor system, i.e., its quick adaptability is restricted to learning a novel sensorimotor mapping, not to persistent sensory bias of bodily property.

The discrete nature of our reaching task may contribute to the persistence of sensory bias. Within-movement corrections indicates that the sensorimotor system learns about sensory bias of mass estimation (Dimitriou et al., 2013), possibly via kinesthetic feedback during movement (Papaxanthis et al., 2005; Proske & Weber, 2023; Weber & Stelzer, 2022). However, movement-related cues only become available after movement initiation. Once a movement ends and the hand returns to rest, microgravity continues to elicit misleading sensory cues that bias mass estimation between trials. This lack of between-trial adaptation parallels findings from a manual interception study aboard the International Space Station, where astronauts persistently initiated movements too early when attempting to intercept an object moving at constant speed (McIntyre et al., 2001). Although astronauts corrected their movements online within each trial, their initial timing error persisted across multiple trials and sessions during a 15-day spaceflight. Hence, discrete motor tasks, such as manual interception and reaching, rely heavily on feedforward control, and are susceptible to sensory biases induced by microgravity. This explains why continuous reaching between targets, without stopping, shows quicker adaptation to zero gravity in parabolic flights (Papaxanthis et al., 2005) and does not exhibit prolonged movement duration during spaceflight (Fowler et al., 2008).

What are the potential consequences of body mass underestimation beyond the simple reaching movements examined here? The implications may be particularly significant given two key considerations. First, the majority of human movements are not deliberately controlled (Brooks, 1986; Marsden et al., 1976), suggesting that underactuated initial movements may be pervasive in microgravity—especially for actions involving larger body masses such as whole-body movements or object manipulation. Without the controlled conditions and explicit speed requirements of our experimental task, such underactuation might manifest even more prominently in natural movements during spaceflight. Second, our finding of increased reliance on feedback-based corrections points to a potentially costly compensatory mechanism. As

feedforward control becomes systematically biased by mass underestimation, the sensorimotor system must depend more heavily on feedback control to achieve adequate performance. This increased reliance on feedback processes may demand additional cognitive resources for action regulation (Bock et al., 2010), potentially contributing to the non-specific stressors that have been shown to impair human performance in space (Tian et al., 2024). The cognitive cost of these compensatory adjustments might be particularly relevant for complex motor tasks or situations requiring divided attention during spaceflight operations.

The preservation of speed-accuracy trade-offs in our study extends previous findings from Fitts' task experiments performed during spaceflight (Fowler et al., 2008). Both the traditional speed-accuracy trade-off and action planning-dependent trade-off remained intact in microgravity (Figure S6), suggesting preserved fundamental motor control capacity. Motor performance during spaceflight typically degrades in tasks with high cognitive demands (Eddy et al., 1998; Manzey et al., 1998; Strangman et al., 2014), particularly those requiring sustained attention (Tian et al., 2024). Our findings suggest that while mass underestimation affects movement execution, the underlying motor control capabilities remain robust in microgravity when cognitive demands are modest.

Our study presents three methodological limitations that warrant consideration. First, despite matching for age and gender, our ground controls exhibited faster movements than the taikonauts. This systematic difference, reflected in higher peak acceleration and speed, may stem from differing experience with the touchpad device used for movement recording. While taikonauts used touchpads regularly, 9 of 12 control participants had minimal experience, potentially leading to compensatory faster movements to avoid overtime errors. Second, the temporal evolution of mass underestimation effects remains unclear. Our earliest measurements occurred three weeks post-launch, though parabolic flight studies suggest these effects may emerge within hours of microgravity exposure (Crevecoeur et al., 2014; Papaxanthis et al.,

2005). Additionally, incomplete post-flight recovery in some kinematic measures suggests either a mass overestimation due to exaggerated weight-related cues or neuromuscular deficiency typically observed shortly after returning to earth (Tays et al., 2021). Third, while our hand-reaching task enabled us to use well-established analytical frameworks for studying motor control aspects of movements, the generalizability of mass underestimation effects to other movements, particularly whole-body actions, remains to be determined. Future research should address these limitations by implementing matched device training protocols, adding early- and post-flight measurements, and extending investigations to diverse motor tasks.

In conclusion, our study provides compelling evidence that movement slowing in microgravity stems from systematic underestimation of body mass, rather than a conservative control strategy. By leveraging the direction-dependent variation in limb effective mass, we demonstrated that reaching movements in microgravity exhibit kinematic signatures—reduced and earlier peak speed/acceleration—that precisely match the predictions of mass underestimation. The persistence of these effects throughout long-duration spaceflight, coupled with increased feedback-based corrections, reveals how altered sensory inputs fundamentally impact both predictive and reactive components of motor control and evades sensorimotor adaptation. While basic motor control capabilities remain intact, as evidenced by preserved speed-accuracy trade-offs, the consistent underactuation of movements may have significant implications for the theorization of sensorimotor learning and for practical considerations of motor performance during space operations. These findings not only advance our understanding of how the sensorimotor system adapts to novel gravitational environments but also reveal fundamental principles of sensorimotor integration, particularly the central role of gravitational cues in shaping our perception of body dynamics.

Methods

Participants. Twelve taikonauts (2 females, 10 males; mean age 49.5 ± 6.5 years) from the first four missions of the China Space Station (CSS) served as the experimental group (Table S1). The control group consisted of 12 right-handed residents from Beijing (2 females, 10 males; mean age 49.9 ± 6.5 years). Control group received monetary compensation. All participants were provided with written informed consent forms, approved by the Ethics Committee of the China Astronaut Research and Training Center and the Institutional Review Board of Peking University. The experimental group was exposed to microgravity for 92–187 days during manned missions in China's Shenzhou Program. Due to operational constraints, the number of test sessions varied among taikonauts: one completed 4 sessions, five completed 6, and six completed 7 (Table S1). All control sessions were conducted at Peking University.

Task and experimental design. The task was conducted using a tablet (Surface Pro 6, Microsoft, Redmond, Washington) and noise-canceling earphones (FiiO FA7, FiiO Electronics Technology, Guangzhou, China). During in-flight sessions, participants wore earphones and assumed a neutral posture with feet secured by foot straps in front of a foldable tabletop, positioned 0.9 meters above the cabin floor. They held the tabletop edge with their left hand, allowing their right hand to move freely on the tablet (Figure 6A). The foot straps and left-hand grip provided body stabilization. The tablet, attached to the tabletop with Velcro, was placed ~35 cm in front of participants and 30 cm below chest level (Figure 6A). At the start of each trial, an orange circle (0.5 cm radius) appeared at the bottom of the screen, signaling participants to move their right index finger to this start circle. After a random delay (500–1000 ms), a target appeared at one of three possible locations, 12 cm from the start circle at 45°, 90°, or 135° counterclockwise from the horizontal axis (Figure 6A). Participants were instructed to reach the target quickly and accurately, pausing briefly before returning to the start. If the time from target appearance to movement end (finger speed <10 cm/s) exceeded 650 ms, a "too slow" message prompted

faster movement. In half of the trials, a 50 ms “beep” sound was played at target appearance. Each session included 120 trials, with 3 target directions and 2 beep conditions balanced and randomized (Figure 6B). The x-y position of the index finger was recorded continuously at 100 Hz.

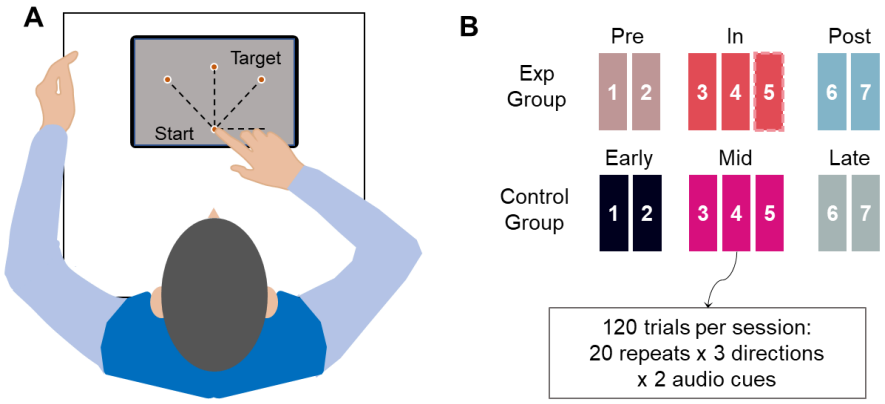

Figure 6. Experimental Setup and Design. A) Top-down view of a participant performing the reaching task with the right hand on a tablet. The start position and all possible target locations are shown as orange dots on the tablet screen. **B)** Experimental design. Both groups completed 4–7 sessions, with each session consisting of 120 trials. Some taikonauts missed 1 or 2 in-flight sessions.

The control group was included to assess a potential confounding effect of repeated measurements. The interval between successive test sessions was 6–9 days, which was shorter than those of the taikonauts (1–2 months) to conservatively evaluate potential practice effects. Despite the shorter intervals, no significant differences were observed across sessions for most measures (except reaction time), confirming minimal practice effects and providing a robust baseline for evaluating microgravity’s impact on the taikonauts. All ground tests, for both groups, were conducted using identical devices and software. The layout of the table and tablet was kept consistent across sessions. The only difference was that, in ground tests, participants

sat in a chair approximately 90 cm above the ground without foot straps and did not need to hold the edge of the tabletop with their left hand for stability.

Data analysis

Kinematic analysis. A Butterworth low-pass filter with a 20 Hz cutoff frequency was applied to the positional data. Movement distance at each time point was computed as the Euclidean distance between the finger's current position and the center of the start circle. Speed was estimated by performing linear regression over a moving window of five consecutive positional data points, and acceleration was calculated similarly from the speed data. Movement onset was defined as the first time point at which acceleration exceeded 50 cm/s², while movement offset was the first time point at which acceleration fell below 50 cm/s². Reaction time was defined as the interval between target onset and movement onset, and movement duration as the interval between movement onset and offset. Movement endpoint error was computed as the Euclidean distance between the target and the finger's position at movement offset. Peak speed and peak acceleration were identified as the maximum speed and acceleration occurring between movement onset and offset, respectively. The times of peak speed and peak acceleration were measured as their respective time intervals from movement onset, and their relative times were calculated by dividing each by the movement duration.

Submovement extraction. To separate the primary submovement from the secondary corrective submovement, the speed profile of each reaching movement was decomposed into a sum of submovements. Following the optimization algorithm described by Rohrer and Hogan (2006), the speed profile was fitted as a sum of support-bounded lognormal (LGNB) curves. Each LGNB curve is defined as:

$$B(t) = \frac{(T_1 - T_0)D}{\sigma\sqrt{2\pi}(t - T_0)(T_1 - t)} exp\left\{\left(\frac{-1}{2\sigma^2}\right)\left[ln\left(\frac{t - T_0}{T_1 - t}\right) - \mu\right]^2\right\},$$

where T_0 and T_1 represent the start and end times of the movement, D is a scaling parameter, and the parameters μ and σ determine the skewness and kurtosis of the underlying lognormal function. These five parameters enable each LGNB submovement to vary across a wide range of possible shapes.

In theory, the number of submovements could be treated as a free parameter. However, to avoid overfitting, we limited each movement to two submovements, given the brevity of the movement (average duration approx. 350 ms). For each trial, we initially fit the data using both one and two LGNB curves and then determined the optimal number of submovements using the "greedy" method from the previous study (Rohrer & Hogan, 2006). Briefly, the fitting error for each movement with one and two LGNB curves was calculated as:

$$\varepsilon = \frac{\int |F(t) - G(t)| dt}{\int |G(t)| dt},$$

where G(t) is the actual movement speed profile, and F(t) is the fitted speed profile (the sum of the submovements). If the fitting error for a single submovement was below a 2% threshold, or if adding a second submovement reduced the fitting error by less than 2%, a single submovement was considered adequate. Otherwise, two submovements were included. Trials with large fitting errors (>10%) were discarded, accounting for 3.60% and 4.83% of trials in the experimental and control groups, respectively. The percentage of trials with two submovements was calculated for each movement direction and phase. The time difference between the peaks of the two submovements was also computed, and set to zero if only one submovement was detected. Data fitting was performed using Matlab's *fmincon* function (MathWorks, Natick, MA, USA), and the robustness of fitting was confirmed by testing 20 random sets of initial parameters.

Statistical analysis. First, invalid trials were excluded from further analysis, with three possible causes: early initiation (RT < 150 ms, indicating guessing of the target direction), affecting

0.74% and 0.70% of trials in the experimental and control groups, respectively; late initiation (RT > 400 ms, indicating inattention), affecting 1.13% and 0%; and measurement failures, affecting 1.16% and 0.70%. The proportion of invalid trials did not differ significantly across testing phases (Friedman's tests, all $p > 0.1$).

Most dependent measures—including movement duration, peak acceleration, peak speed, time to peak acceleration/speed, relative time to peak acceleration/speed, the percentage of submovements, and inter-peak intervals—were analyzed using two-way repeated-measures ANOVAs with a 3 (phase) × 3 (movement direction) design. Reaction time was analyzed using three-way repeated-measures ANOVAs with a 3 (phase) × 3 (movement direction) × 2 (beep/no beep) design. Greenhouse-Geisser corrections were applied when sphericity was violated (Kirk, 1968). Normality was assessed with Shapiro-Wilk tests, and if more than 10% of tests for a dependent variable violated normality, the Aligned Rank Transform (ART) procedure was applied before conducting repeated-measures ANOVA. Tukey's HSD tests were used for pairwise comparisons.

To examine the relationship between submovement and movement duration, a Linear Mixed Model (LMM) was used to analyze the association between changes in the inter-peak interval of submovements (ΔIPI) and changes in movement duration (ΔMD). The dependent variable $y_{\Delta MD}$ represents the mean change in movement duration across two adjacent phases (pre-to-in and post-to-in transitions) for each target direction. Target direction (45°, 90°, 135°) and phase transitions (pre-to-in and post-to-in) were treated as within-subject factors. The predictors included three fixed factors: ΔIPI, phase transition (x_{pha}), and direction (x_{dir}). An intercept term (u_{par}) was included as a random factor to account for individual differences in movement duration. The resulting LMM is as follows:

$$y_{\Delta MD} = \beta_0 + \beta_1 x_{\Delta IPI} + \beta_2 x_{pha} + \beta_3 x_{dir} + Zu_{par} + \varepsilon,$$

where β_0 denotes the overall intercept and ε denotes a Gaussian residual error.

All statistical analyses were performed using MATLAB's Statistics and Machine Learning Toolbox. The significance level was set at $\alpha = 0.05$, and all tests were two-tailed unless otherwise specified.

Acknowledgements: We would like to thank Mr. Shaolin Zeng for his help with data acquisition of the control group. **Funding:** This work was supported by STI2030-Major Projects (2021ZD0202600), the Space Medical Experiment Project of China Manned Space Program (HYZHXM03002, HYZHXMR01001) and the National Natural Science Foundation of China (62061136001, 32071047, 31871102), awarded to KW; the National Natural Science Foundation of China (32300868) awarded to ZZ; the Foundation of National Key Laboratory of Human Factors Engineering (HFNKL2023J02) to awarded to YT; and the the National Key Research and Development Program of China under Grant (2023YFF1203905) to awarded to CW. **Authors contributions:** Conceptualization: KW, YT, ZZ; Data curation: YT, ZZ; Formal analysis: ZZ; Funding acquisition: KW, CW, YT, ZZ; Methodology: KW, ZZ; Software: YT, CW, CJ, BW, HY, RZ; Supervision: KW; Visualization: ZZ; Writing: KW, ZZ.

Competing interests: Authors declare that they have no competing interests.

Data and materials availability: Experimental data of the control group will be made available upon reasonable request.

References

Berger, M., Mescheriakov, S., Molokanova, E., Lechner-Steinleitner, S., Seguer, N., & Kozlovskaya, I. (1997). Pointing arm movements in short- and long-term spaceflights. *Aviation, Space, and Environmental Medicine*, *68*(9), 781–787.

Berniker, M., & Kording, K. (2008). Estimating the sources of motor errors for adaptation and generalization. *Nature Neuroscience*, *11*(12), 1454–1461.

Bock, O. (1998). Problems of sensorimotor coordination in weightlessness. *Brain Research. Brain Research Reviews*, *28*(1-2), 155–160.

Bock, O., Arnold, K. E., & Cheung, B. S. (1996a). Performance of a simple aiming task in hypergravity: II. detailed response characteristics. *Aviation, Space, and Environmental Medicine*, *67*(2), 133–138.

Bock, O., Arnold, K. E., & Cheung, B. S. (1996b). Performance of a simple aiming task in hypergravity: I. overall accuracy. *Aviation, Space, and Environmental Medicine*, *67*(2), 127–132.

Bock, O., Fowler, B., & Comfort, D. (2001). Human sensorimotor coordination during spaceflight: an analysis of pointing and tracking responses during the “Neurolab” Space Shuttle mission. *Aviation, Space, and Environmental Medicine*, *72*(10), 877–883.

Bock, O., Fowler, B., Jüngling, S., & Comfort, D. (2003). Visual-motor coordination during spaceflight. *The Neurolab Space Mission: Neuroscience Research in Space. Houston, Tx*, 83–89.

Bock, O., Howard, I. P., Money, K. E., & Arnold, K. E. (1992). Accuracy of aimed arm movements in changed gravity. *Aviation, Space, and Environmental Medicine*, *63*(11), 994–998.

Bock, O., Weigelt, C., & Bloomberg, J. J. (2010). Cognitive demand of human sensorimotor performance during an extended space mission: a dual-task study. *Aviation, Space, and*

Environmental Medicine, *81*(9), 819–824.

Brooks, V. B. (1986). The neural basis of motor control: Oxford University Press. In *Oxford*.

Chua, R., & Elliott, D. (1993). Visual regulation of manual aiming. *Human Movement Science*, *12*(4), 365–401.

Craik, K. J. W. (1947). Theory of the human operator in control systems; the operator as an engineering system. *The British Journal of Psychology. General Section*, *38*(Pt 2), 56–61.

Crevecoeur, F., McIntyre, J., Thonnard, J.-L., & Lefèvre, P. (2010). Movement stability under uncertain internal models of dynamics. *Journal of Neurophysiology*, *104*(3), 1301–1313.

Crevecoeur, F., McIntyre, J., Thonnard, J.-L., & Lefèvre, P. (2014). Gravity-dependent estimates of object mass underlie the generation of motor commands for horizontal limb movements. *Journal of Neurophysiology*, *112*(2), 384–392.

Dimitriou, M., Wolpert, D. M., & Franklin, D. W. (2013). The temporal evolution of feedback gains rapidly update to task demands. *The Journal of Neuroscience: The Official Journal of the Society for Neuroscience*, *33*(26), 10898–10909.

Eddy, D. R., Schiflett, S. G., Schlegel, R. E., & Shehab, R. L. (1998). Cognitive performance aboard the life and microgravity spacelab. *Acta Astronautica*, *43*(3-6), 193–210.

Elliott, D., Hansen, S., Grierson, L. E. M., Lyons, J., Bennett, S. J., & Hayes, S. J. (2010). Goal-directed aiming: two components but multiple processes. *Psychological Bulletin*, *136*(6), 1023–1044.

Elliott, D., Lyons, J., Hayes, S. J., Burkitt, J. J., Roberts, J. W., Grierson, L. E. M., Hansen, S., & Bennett, S. J. (2017). The multiple process model of goal-directed reaching revisited. *Neuroscience and Biobehavioral Reviews*, *72*, 95–110.

Fercho, K., & Baugh, L. A. (2014). It's too quick to blame myself—the effects of fast and slow rates of change on credit assignment during object lifting. *Frontiers in Human Neuroscience*, *8*. https://doi.org/10.3389/fnhum.2014.00554

Flanagan, J. R., & Wing, A. M. (1997). The role of internal models in motion planning and

control: evidence from grip force adjustments during movements of hand-held loads. *The Journal of Neuroscience: The Official Journal of the Society for Neuroscience*, *17*(4), 1519–1528.

Flash, T., & Hogan, N. (1985). The coordination of arm movements: an experimentally confirmed mathematical model. *The Journal of Neuroscience: The Official Journal of the Society for Neuroscience*, *5*(7), 1688–1703.

Fowler, B., Meehan, S., & Singhal, A. (2008). Perceptual-motor performance and associated kinematics in space. *Human Factors*, *50*(6), 879–892.

Heuer, H., Manzey, D., Lorenz, B., & Sangals, J. (2003). Impairments of manual tracking performance during spaceflight are associated with specific effects of microgravity on visuomotor transformations. *Ergonomics*, *46*(9), 920–934.

Johansson, R., & Edin, B. (1993). Predictive feed-forward sensory control during grasping and manipulation in man. *Biomedical Research-Tokyo*, *14*, 95–106.

Kanas, N., & Manzey, D. (2008). Basic Issues of Human Adaptation to Space Flight. In *Space Psychology and Psychiatry* (pp. 15–48). Springer Netherlands.

Kawato, M. (1999). Internal models for motor control and trajectory planning. *Current Opinion in Neurobiology*, *9*(6), 718–727.

Kirk, R. (1968). *Experimental design: Procedures for the behavioral sciences* (Vol. 1–f). Brooks/Cole.

Kluzik, J., Diedrichsen, J., Shadmehr, R., & Bastian, A. J. (2008). Reach adaptation: what determines whether we learn an internal model of the tool or adapt the model of our arm? *Journal of Neurophysiology*, *100*(3), 1455–1464.

Kong, G., Zhou, Z., Wang, Q., Kording, K., & Wei, K. (2017). Credit assignment between body and object probed by an object transportation task. *Scientific Reports*, *7*(1), 13415.

Krakauer, J. W., Hadjiosif, A. M., Xu, J., Wong, A. L., & Haith, A. M. (2019). Motor learning. *Comprehensive Physiology*, *9*(2), 613–663.

Krakauer, J. W., Pine, Z. M., Ghilardi, M. F., & Ghez, C. (2000). Learning of visuomotor transformations for vectorial planning of reaching trajectories. *Journal of Neuroscience*, *20*(23), 8916–8924.

Kubis, J. F., Mclaughlin, E. J., Jackson, J. M., Rusnak, R., Mcbride, G. H., & Saxon, S. V. (1977). Task and work performance on Skylab missions 2, 3, and 4: Time and motion study: Experiment M151. *NASA. JSC Biomed. Results from Skylab*. https://ntrs.nasa.gov/citations/19770026852

Kurtzer, I. L., Pruszynski, J. A., & Scott, S. H. (2008). Long-latency reflexes of the human arm reflect an internal model of limb dynamics. *Current Biology: CB*, *18*(6), 449–453.

Lackner, J. R., & DiZio, P. (1992). Gravitoinertial force level affects the appreciation of limb position during muscle vibration. *Brain Research*, *592*(1-2), 175–180.

Lackner, J. R., & Dizio, P. (1994). Rapid adaptation to Coriolis force perturbations of arm trajectory. *Journal of Neurophysiology*, *72*(1), 299–313.

Layne, C. S., Mulavara, A. P., McDonald, P. V., Pruett, C. J., Kozlovskaya, I. B., & Bloomberg, J. J. (2001). Effect of long-duration spaceflight on postural control during self-generated perturbations. *Journal of Applied Physiology*, *90*(3), 997–1006.

Li, W., & Todorov, E. (2004). Iterative linear quadratic regulator design for nonlinear biological movement systems. *First International Conference on Informatics in*. https://www.scitepress.org/PublishedPapers/2004/11439/

Manzey, D., Lorenz, B., & Poljakov, V. (1998). Mental performance in extreme environments: results from a performance monitoring study during a 438-day spaceflight. *Ergonomics*, *41*(4), 537–559.

Marsden, C. D., Merton, P. A., & Morton, H. B. (1976). Stretch reflex and servo action in a variety of human muscles. *The Journal of Physiology*, *259*(2), 531–560.

McIntyre, J., Zago, M., Berthoz, A., & Lacquaniti, F. (2001). Does the brain model Newton's laws? *Nature Neuroscience*, *4*(7), 693–694.

Mechtcheriakov, S., Berger, M., Molokanova, E., Holzmueller, G., Wirtenberger, W., Lechner-Steinleitner, S., De Col, C., Kozlovskaya, I., & Gerstenbrand, F. (2002). Slowing of human arm movements during weightlessness: the role of vision. *European Journal of Applied Physiology*, *87*(6), 576–583.

Meyer, D. E., Abrams, R. A., Kornblum, S., Wright, C. E., & Smith, J. E. (1988). Optimality in human motor performance: ideal control of rapid aimed movements. *Psychological Review*, *95*(3), 340–370.

Meyer, D. E., Keith Smith, J. E., Kornblum, S., Abrams, R., & Wright, C. (2018). Speed—accuracy tradeoffs in aimed movements: Toward a theory of rapid voluntary action. *Attention and Performance XIII*. https://doi.org/10.4324/9780203772010-6

Mussa-Ivaldi, F. A., Hogan, N., & Bizzi, E. (1985). Neural, mechanical, and geometric factors subserving arm posture in humans. *The Journal of Neuroscience: The Official Journal of the Society for Neuroscience*, *5*(10), 2732–2743.

Newman, D. J., & Lathan, C. E. (1999). Memory processes and motor control in extreme environments. *IEEE Transactions on Systems, Man and Cybernetics. Part C, Applications and Reviews: A Publication of the IEEE Systems, Man, and Cybernetics Society*, *29*(3), 387–394.

Paloski, W. H., Reschke, M. F., Black, F. O., & Dow, R. S. (1999). *Recovery of postural equilibrium control following space flight* (No. DSO-605). ntrs.nasa.gov. https://ntrs.nasa.gov/citations/20040201535

Papaxanthis, C., Pozzo, T., & McIntyre, J. (2005). Kinematic and dynamic processes for the control of pointing movements in humans revealed by short-term exposure to microgravity. *Neuroscience*, *135*(2), 371–383.

Papaxanthis, C., Pozzo, T., Popov, K. E., & McIntyre, J. (1998). Hand trajectories of vertical arm movements in one-G and zero-G environments. Evidence for a central representation of gravitational force. *Experimental Brain Research. Experimentelle Hirnforschung.*

Experimentation Cerebrale, *120*(4), 496–502.

Plamondon, R., & Alimi, A. M. (1997). Speed/accuracy trade-offs in target-directed movements. *The Behavioral and Brain Sciences*, *20*(02), 279–303.

Proske, U., & Gandevia, S. C. (2012). The proprioceptive senses: their roles in signaling body shape, body position and movement, and muscle force. *Physiological Reviews*, *92*(4), 1651–1697.

Proske, U., & Weber, B. M. (2023). Proprioceptive disturbances in weightlessness revisited. *NPJ Microgravity*, *9*(1), 64.

Reschke, M. F., Bloomberg, J. J., Harm, D. L., Paloski, W. H., Layne, C., & McDonald, V. (1998). Posture, locomotion, spatial orientation, and motion sickness as a function of space flight. *Brain Research. Brain Research Reviews*, *28*(1-2), 102–117.

Rohrer, B., & Hogan, N. (2006). Avoiding spurious submovement decompositions II: a scattershot algorithm. *Biological Cybernetics*, *94*(5), 409–414.

Ross, H. E., & Reschke, M. F. (1982). Mass estimation and discrimination during brief periods of zero gravity. *Perception & Psychophysics*, *31*(5), 429–436.

Sangals, J., Heuer, H., Manzey, D., & Lorenz, B. (1999). Changed visuomotor transformations during and after prolonged microgravity. *Experimental Brain Research. Experimentelle Hirnforschung. Experimentation Cerebrale*, *129*(3), 378–390.

Shadmehr, R., Huang, H. J., & Ahmed, A. A. (2016). A Representation of Effort in Decision-Making and Motor Control. *Current Biology: CB*, *26*(14), 1929–1934.

Shadmehr, R., & Mussa-Ivaldi, F. A. (1994). Adaptive representation of dynamics during learning of a motor task. *Journal of Neuroscience*, *14*(5), 3208–3224.

Smeets, J. B., & Brenner, E. (1995). Prediction of a moving target's position in fast goal-directed action. *Biological Cybernetics*, *73*(6), 519–528.

Strangman, G. E., Sipes, W., & Beven, G. (2014). Human cognitive performance in spaceflight and analogue environments. *Aviation, Space, and Environmental Medicine*, *85*(10),

1033–1048.

Sutter, K., Oostwoud Wijdenes, L., van Beers, R. J., & Medendorp, W. P. (2021). Movement preparation time determines movement variability. *Journal of Neurophysiology*, *125*(6), 2375–2383.

Tafforin, C., Thon, B., Guell, A., & Campan, R. (1989). Astronaut behavior in an orbital flight situation: preliminary ethological observations. *Aviation, Space, and Environmental Medicine*, *60*(10 Pt 1), 949–956.

Tays, G. D., Hupfeld, K. E., McGregor, H. R., Salazar, A. P., De Dios, Y. E., Beltran, N. E., Reuter-Lorenz, P. A., Kofman, I. S., Wood, S. J., Bloomberg, J. J., Mulavara, A. P., & Seidler, R. D. (2021). The Effects of Long Duration Spaceflight on Sensorimotor Control and Cognition. *Frontiers in Neural Circuits*, *15*, 723504.

Tian, Y., Zhang, Z., Jiang, C., Chen, D., Liu, Z., Wei, M., Wang, C., & Wei, K. (2024). Stressors affect human motor timing during spaceflight. *NPJ Microgravity*, *in press*.

Todorov, E. (2004). Optimality principles in sensorimotor control. *Nature Neuroscience*, *7*(9), 907.

Todorov, E. (2005). Stochastic optimal control and estimation methods adapted to the noise characteristics of the sensorimotor system. *Neural Computation*, *17*(5), 1084–1108.

Wang, J., & Sainburg, R. L. (2004). Interlimb transfer of novel inertial dynamics is asymmetrical. *Journal of Neurophysiology*, *92*(1), 349–360.

Weber, B., Riecke, C., & Stelzer, M. (2019). *Disentangling the enigmatic slowing effect of microgravity on sensorimotor performance*. HFES-Europe.

Weber, B., & Stelzer, M. (2022). Sensorimotor impairments during spaceflight: Trigger mechanisms and haptic assistance. *Frontiers in Neuroergonomics*, *3*, 959894.

Wilke, C., Synofzik, M., & Lindner, A. (2013). Sensorimotor recalibration depends on attribution of sensory prediction errors to internal causes. *PloS One*, *8*(1), e54925.

Wolpert, D. M., Diedrichsen, J., & Flanagan, J. R. (2011). Principles of sensorimotor learning.

Nature Reviews. Neuroscience, *12*(12), 739.

Wolpert, D. M., Ghahramani, Z., & Jordan, M. I. (1995). An internal model for sensorimotor integration. *Science*, *269*(5232), 1880–1882.

Wolpert, D. M., & Miall, R. C. (1996). Forward models for physiological motor control. *Neural Networks: The Official Journal of the International Neural Network Society*, *9*(8), 1265–1279.

Wolpert, D. M., Miall, R. C., & Kawato, M. (1998). Internal models in the cerebellum. *Trends in Cognitive Sciences*, *2*(9), 338–347.

Woodworth, R. S. (1899). Accuracy of voluntary movement. *Psychological Monographs*, *3*(3), i – 114.

Supplemental Materials

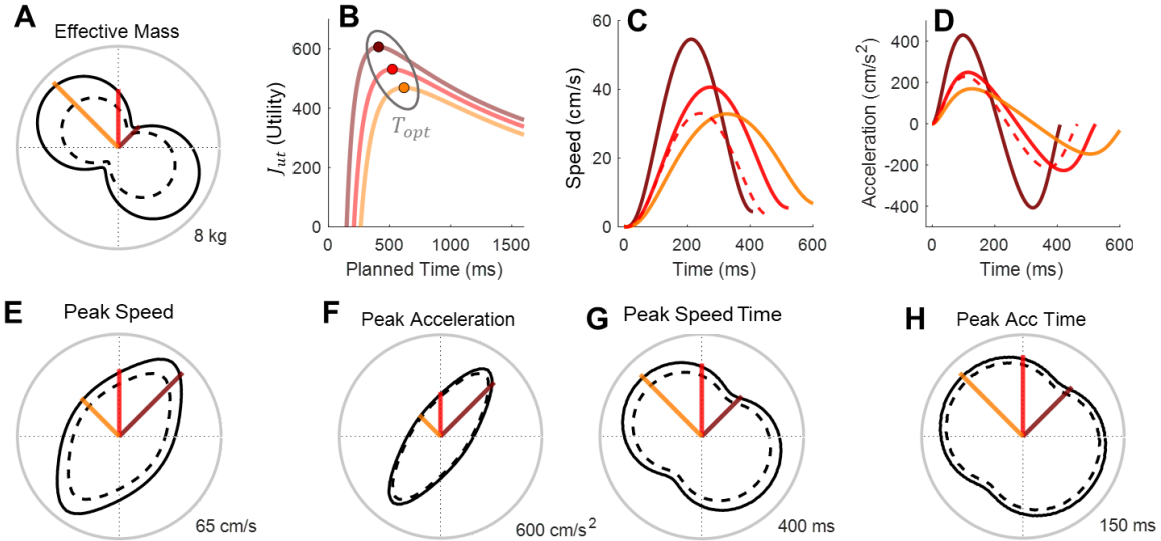

Figure S1. Simulation details for the arm model. A) Effective mass across different movement directions, with three colored lines indicating the specific directions used in the experiment. The solid-line contour denotes the effective mass simulated by default parameters under normal gravity (see Supplemental Text 1), and the dash-line contour denotes a hypothetical 30% underestimation of the effective mass in microgravity **B)** Utility function values for movements in each of the three directions. **C-D)** Speed and acceleration profiles for movements in these directions. **E-H)** Simulated values of peak speed, peak acceleration, peak speed timing, and peak acceleration timing across all movement directions. The solid-line contours denote simulated values by default parameters, and the dash-line contours denotes the values with a 30% mass underestimation.

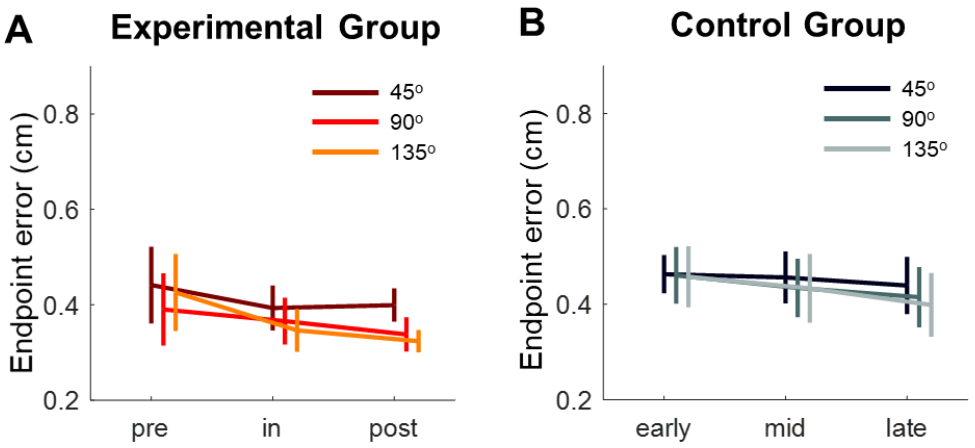

Figure S2. **Movement accuracy quantified by endpoint error.** The average endpoint error for each target was analyzed across experimental phases. Both the experimental group **A)** and control group **B)** performed the task with high accuracy despite the stringent timing requirements. The presence of a beep had no effect on endpoint error in either group (experimental group: main effect, $F(1,11) = 1.4461$, $p = 0.254$; all interactions, $p > 0.2$; control group: main effect, $F(1,11) = 0.717$, $p = 0.415$; all interactions, $p > 0.25$). Therefore, data from the two beep conditions were pooled, and a two-way repeated-measures ANOVA was conducted for each group. In the experimental group, endpoint error showed a slight decrease across phases, but the main effect of phase was not statistically significant ($F(2,22) = 1.768$, $p = 0.210$), nor was the interaction effect ($F(2,22) = 2.386$, $p = 0.091$). However, there was a significant main effect of direction ($F(2,22) = 16.020$, $p < 0.001$, partial $\eta^2 = 0.593$), with post-hoc comparisons revealing that the 45° direction had significantly larger endpoint errors than the 90° and 135° directions ($p = 0.002$, partial $\eta^2 = 0.291$; $p = 0.001$, partial $\eta^2 = 0.286$, respectively). In the control group, no significant effects of phase or direction were observed, and there was no significant interaction (all $p > 0.23$).

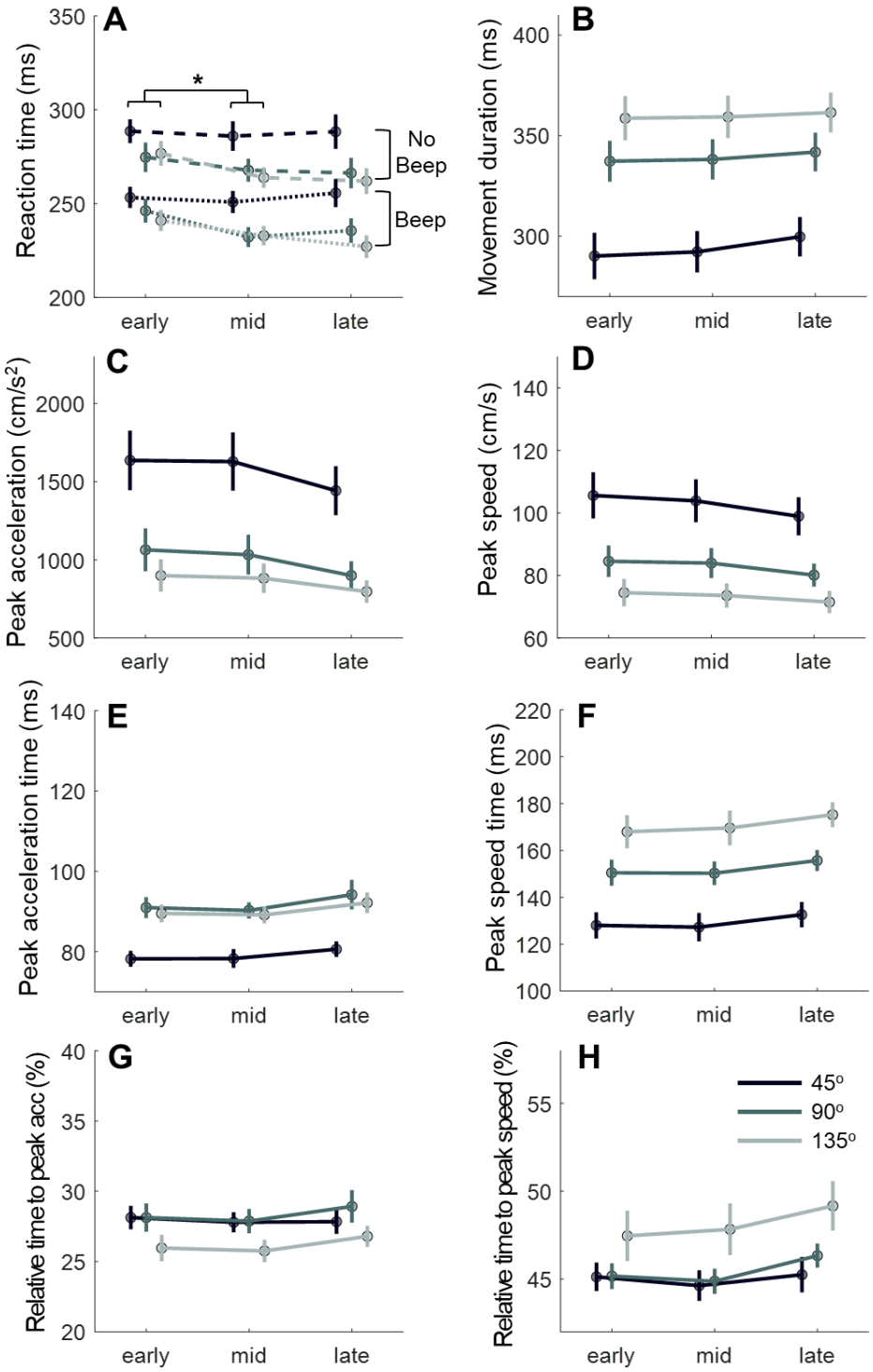

Figure S3. Results of kinematic analysis of the control group. The control group exhibited no phase effect for most performance measures, with the exception of reaction time (RT).

However, similar effects were also observed in the experimental group. Each measure was analyzed using a 3 (direction) × 3 (phase) two-way repeated-measures ANOVA. **A)** Reaction Time (RT): Significant main effects of direction ($F(2,22) = 21.946$, $p < 0.001$, partial $\eta^2 = 0.666$) and phase ($F(2,22) = 4.281$, $p = 0.039$, partial $\eta^2 = 0.280$) were found, along with a significant direction-phase interaction ($F(2,22) = 7.940$, $p = 0.001$, partial $\eta^2 = 0.419$). RT was significantly faster in the Middle phase than in the Early phase ($p = 0.032$, D = 0.285). **B)** Movement Duration (MD): Significant main effect of direction ($F(2,22) = 99.874$, $p < 0.001$, partial $\eta^2 = 0.901$), with all pairwise comparisons significant at $p < 0.001$. Neither main effect of phase ($F(2,22) = 0.995$, $p = 0.360$) nor interaction effect ($F(4,44) = 1.412$, $p = 0.114$) was significant. **C)** Peak acceleration: Significant main effect of direction ($F(2,22) = 55.460$, $p < 0.001$, partial $\eta^2 = 0.834$), with all pairwise comparisons significant at $p < 0.001$. A marginal phase effect ($F(2,22) = 3.462$, $p = 0.081$) and interaction ($F(4,44) = 2.715$, $p = 0.067$) were noted. **D)** Peak speed: Significant main effect of direction ($F(2,22) = 66.071$, $p < 0.001$, partial $\eta^2 = 0.857$), with all pairwise comparisons significant at $p < 0.001$. No phase effect ($F(2,22) = 2.360$, $p = 0.148$) or interaction ($F(4,44) = 1.975$, $p = 0.145$) was observed. **E)** Peak acceleration time: Significant main effect of direction ($F(2,22) = 26.602$, $p < 0.001$, partial $\eta^2 = 0.707$). No phase effect ($F(2,22) = 1.440$, $p = 0.260$) or interaction ($F(4,44) = 0.132$, $p = 0.900$) was observed. Pairwise comparisons showed significantly shorter times for 45° compared to 90° ($p < 0.001$, D = 0.305) and 135° ($p < 0.001$, D = 0.269). **F)** Peak speed time: Significant main effect of direction ($F(2,22) = 96.575$, $p < 0.001$, partial $\eta^2 = 0.898$), with all pairwise comparisons significant at $p < 0.001$. Marginal phase effect ($F(2,22) = 2.702$, $p = 0.098$), and no interaction effect ($F(4,44) = 0.420$, $p = 0.710$). **G)** Relative peak acceleration time: Significant main effect of direction ($F(2,22) = 8.506$, $p = 0.003$, partial $\eta^2 = 0.436$), with no phase effect ($F(2,22) = 1.143$, $p = 0.317$) or interaction ($F(4,44) = 1.002$, $p = 0.381$). Pairwise comparisons indicated that relative peak acceleration time appeared significantly earlier in the 135° direction than in 90° ($p = 0.002$, D = 0.313) and 45° ($p = 0.021$, D = 0.256). **H)** Relative peak speed time: Significant main effect of direction ($F(2,22) = 6.779$, $p = 0.007$, partial $\eta^2 = 0.381$), with a marginal phase effect ($F(2,22) = 2.636$, $p = 0.095$) and no interaction ($F(4,44) = 1.788$, $p = 0.175$). Pairwise comparisons showed that relative peak speed time was significantly earlier in the 135° direction than in 90° ($p = 0.037$, D = 0.264) and 45° ($p = 0.029$, D = 0.308).

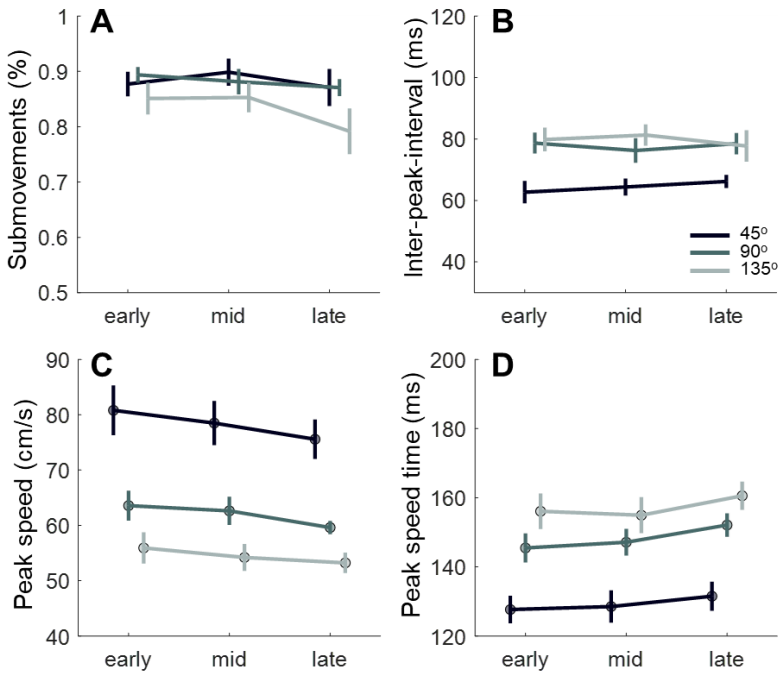

Figure S4. Results of submovement analysis of the control group. All measures of submovements did not show significant phase effect. **A)** Percentage of trials with two submovements. Only a marginal main effect of direction was detected ($F(2,22) = 3.358$, $p = 0.055$, partial $\eta^2 = 0.234$) without a phase effect ($F(2,22) = 2.216$, $p = 0.155$) or interaction ($F(4,44) = 1.209$, $p = 0.320$). **B)** Inter-peak interval (IPI) showed a significant main effect of direction ($F(2,22) = 19.277$, $p < 0.001$, partial $\eta^2 = 0.637$), with no phase effect ($F(2,22) = 0.029$, $p = 0.902$) or interaction ($F(4,44) = 2.028$, $p = 0.134$). Pairwise comparisons indicated a significantly shorter IPI in the 45° direction compared to the other two directions (45° vs. 90°: $p < 0.001$, D = 0.269; 45° vs. 135°: $p = 0.002$, D = 0.305). **C)** Peak speed of the primary submovement exhibited a significant main effect of direction ($F(2,22) = 60.089$, $p < 0.001$, partial $\eta^2 = 0.845$), without a phase effect ($F(2,22) = 2.628$, $p = 0.120$) or interaction ($F(4,44) = 0.949$, $p = 0.420$). Pairwise comparisons showed significant differences between all directions (45° vs. 90°: $p < 0.001$, D = 0.224; 45° vs. 135°: $p < 0.001$, D = 0.326; 90° vs. 135°: $p < 0.001$, D = 0.102). **D)** Peak speed time of the primary submovement revealed a significant main effect of direction ($F(2,22) = 46.259$, $p < 0.001$, partial $\eta^2 = 0.808$), with no phase effect ($F(2,22) = 2.335$, $p = 0.134$) or interaction ($F(4,44) = 0.425$, $p = 0.660$). Pairwise comparisons showed a significantly smaller peak speed time in the 45° direction compared to the other two directions (45° vs. 90°: $p < 0.001$, D = 0.260; 45° vs. 135°: $p < 0.001$, D = 0.311).

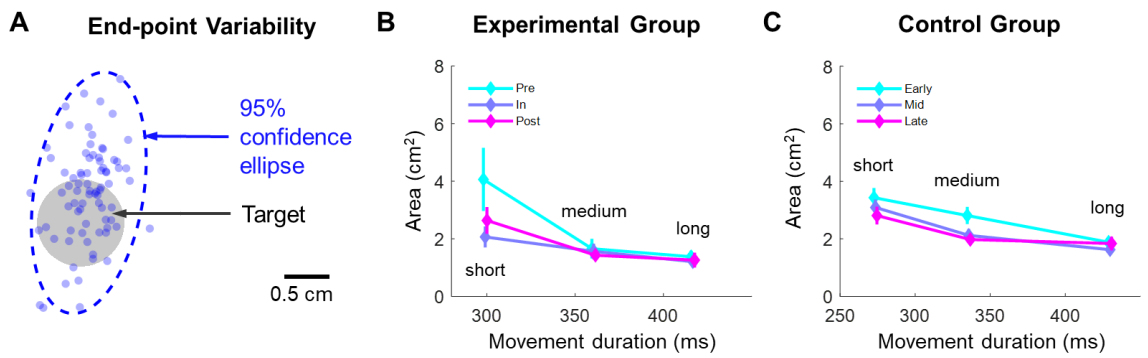

Figure S5. Speed-accuracy trade-off as indicated by the relationship between movement duration (MD) and endpoint dispersion, following the classical Fitts' law. A) Endpoint dispersion was estimated by constructing a 95% confidence ellipse encompassing the endpoints of all trials. Regardless of movement direction, phase, and beep condition, trials were divided into three equal-sized bins based on duration, labeled as short, medium, and long. For each participant at each phase, trials within each bin were pooled to estimate the ellipse of endpoints. **B-C)** A positive association between endpoint area and MD was observed, indicating a speed-accuracy trade-off. Both groups exhibited a dependency of the endpoint area on MD. For the experimental group, a 3 (phase) × 3 (MD) two-way repeated-measures ANOVA on endpoint area showed a significant main effect of MD ($F(2,22) = 14.125$, $p = 0.003$, partial $\eta^2 = 0.407$), with only a marginal phase effect and no interaction (phase: $F(2,22) = 3.199$, $p = 0.087$; interaction: $F(4,44) = 2.106$, $p = 0.163$). Pairwise comparisons indicated that short, medium, and long MD conditions significantly differed from each other (short vs. medium: $p = 0.018$, D = 0.576; medium vs. long: $p = 0.007$, D = 0.113; short vs. long: $p = 0.004$, D = 0.689). The control group yielded similar ANOVA results, with a significant main effect of MD ($F(2,22) = 34.058$, $p < 0.001$, partial $\eta^2 = 0.756$; all post-hoc comparisons were significant at $p < 0.007$). Additionally, the control group exhibited a main effect of phase ($F(2,22) = 9.359$, $p = 0.003$, partial $\eta^2 = 0.460$) without interaction ($F(2,22) = 2.026$, $p = 0.151$, partial $\eta^2 = 0.156$). Post-hoc comparisons revealed that the early phase had a significantly larger area than the middle and late phases (early vs. middle: $p = 0.004$, D = 0.263; early vs. late: $p = 0.018$, D = 0.309). Thus, both groups appear to slightly improve their speed-accuracy trade-off over repeated tests, with no evidence suggesting that spaceflight adversely affects this trade-off.

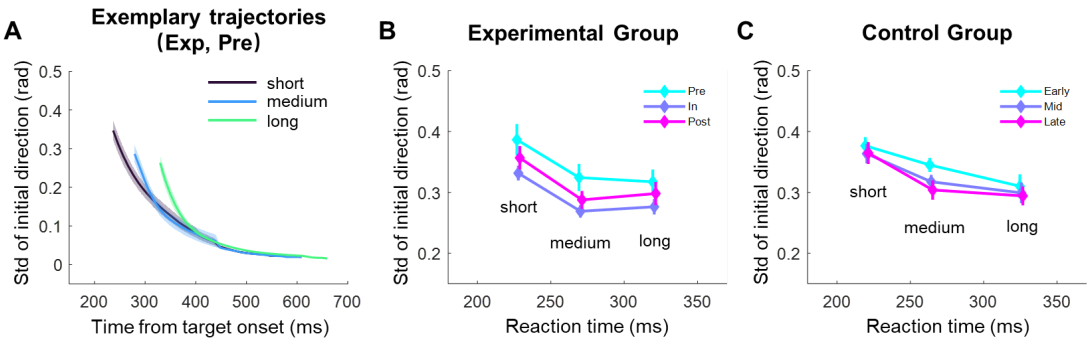

Figure S6. Speed-accuracy trade-off in action planning, illustrated by the relationship between reaction time (RT) and the variance in initial movement direction. A) Similar to the speed-accuracy trade-off analysis in Figure S5, all trials were grouped into three equal-sized bins based on RT, regardless of phase, movement direction, or beep condition. The standard deviation of movement direction is shown over time for these bins, using data from the experimental group in the pre-flight phase as an example. The standard deviation decreases over time within a reaching movement, with shorter RTs resulting in greater directional variance, particularly in the early phase of movement. **B-C)** The standard deviation of initial movement direction as a function of RT, plotted separately for the three phases. A negative trend between standard deviation and RT indicates a speed-accuracy trade-off in action planning. However, phase did not affect the relationship between RT and initial variance. For the experimental group, a 3 (phase) × 3 (RT) two-way repeated measures ANOVA on the standard deviation showed a significant main effect of RT ($F(2,22) = 7.542$, $p = 0.009$, partial $\eta^2 = 0.407$), while neither the main effect of phase nor the interaction was significant (phase: $F(2,22) = 3.160$, $p = 0.083$; interaction: $F(4,44) = 0.503$, $p = 0.694$). Pairwise comparisons indicated that the initial variance of short-RT trials was significantly higher than that of medium-RT trials ($p = 0.004$, $D = 0.375$), while the difference between medium- and long-RT trials was only marginally significant ($p = 0.076$). The control group showed similar results (RT: $F(2,22) = 4.268$, $p = 0.040$, partial $\eta^2 = 0.280$; phase: $F(2,22) = 1.657$, $p = 0.215$; interaction: $F(2,22) = 0.007$, $p = 0.998$). Thus, while clear indications of a speed-accuracy trade-off in action planning were observed, there was no evidence that microgravity negatively affected this relationship.

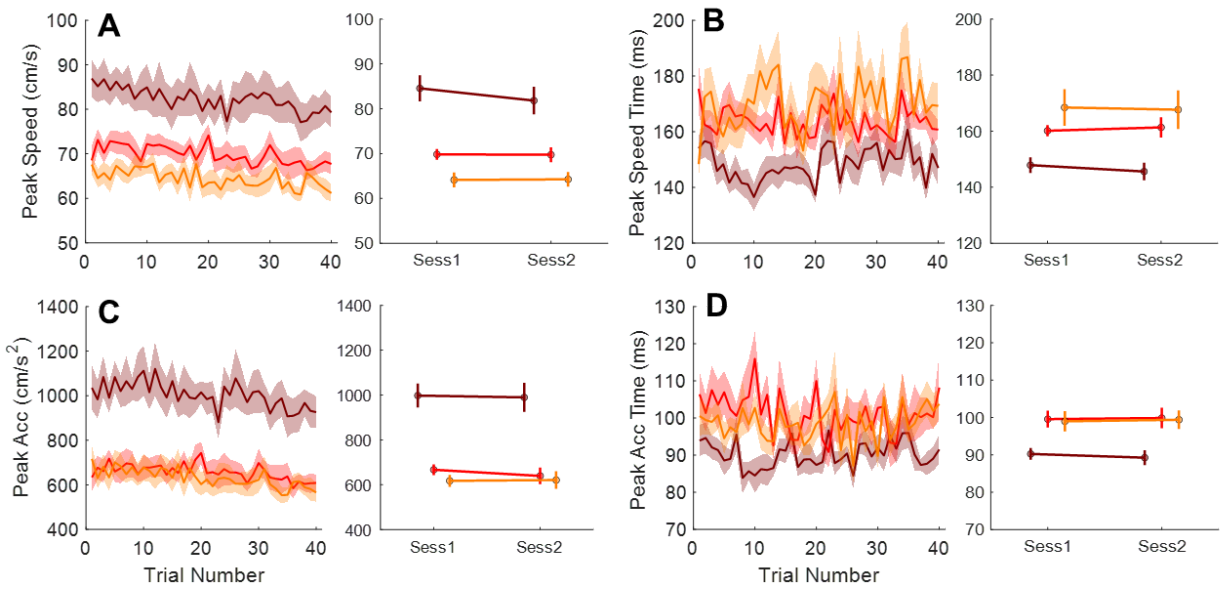

Figure S7. Changes in key performance measures over trials within and between in-flight sessions. To show a lack of within-session and between-session adaptation during spaceflight, we analyzed changes in peak speed **(A)**, peak speed timing of the primary submovement **(B)**, peak acceleration **(C)**, and peak acceleration timing **(D)** across the first and second sessions, as well as trials within the second in-flight session. The second session was specifically analyzed because the sensorimotor system undergoes recalibration during early flight and thus the first session is less likely to show good within-session adaptation. The third session had fewer participants (only six taikonauts). Participant S2, who completed only one in-flight session, was excluded from this analysis. For the within-session analysis, we compared the mean values of the first and last five trials for each measure across movement directions. No significant changes were observed in peak speed timing and peak acceleration timing (all *p*-values > 0.06; panels B and D). Peak speed (panel A) showed a slight and marginally significant decrease in the 45° and 90° directions (45°: from 85.9 ± 3.4 cm/s to 78.5 ± 3.4 cm/s, $p = 0.013$; 90°: from 71.6 ± 2.1 cm/s to 67.3 ± 1.8 cm/s, p = 0.052), but no significant change in the 135° direction ($p = 0.200$). Similarly, peak acceleration (panel C) decreased slightly across all directions with marginal significance (45°: from 1033.9 ± 73.4 cm/s² to 919.9 ± 66.8 cm/s², $p = 0.056$; 90°: from 671.8 ± 43.4 cm/s² to 603.7 ± 33.8 cm/s², $p = 0.097$; 135°: from 663.2 ± 46.3 cm/s² to 586.2 ± 36.2 cm/s², $p = 0.049$). For comparisons between the first and second sessions, we applied a two-way repeated measures ANOVA to these dependent variables and found no significant differences between sessions (all *p*-values > 0.144). These findings suggest that the mass underestimation effects persist over repetitive reaching attempts (120 trials) and practice

sessions. Instead of showing between-trial or between-session adaptation, these effects tend to increase slightly across trials.

Table S1. The schedule of experiment sessions.

Taikonauts	Pre-flight		In-flight			Post-flight	
S1	-43	-24	39	74	--	14	66
S2	-43	-24	39	--	--	14	--
S3	-43	-24	39	74	--	14	66
S4	-157	-60	32	96	131	18	73
S5	-165	-60	32	96	131	18	73
S6	-165	-60	32	96	131	18	73
S7	-31	-12	20	109	--	15	64
S8	-31	-12	20	109	--	15	64
S9	-31	-12	20	109	--	15	64
S10	-91	-48	28	76	125	16	93
S11	-91	-50	28	77	125	16	93
S12	-91	-52	28	76	125	16	93

Numbers in the table represent days before launch (pre-flight), days after launch (in-flight), and days after landing (post-flight).

Supplementary Note 1. Model simulation for illustrating the effect of effective mass on reaching kinematics

We simulated the peak speed, peak acceleration, and their corresponding times for reaching movements in different directions. We employed the classical two-joint arm model to demonstrate the effect of biomechanics ((Li & Todorov, 2004); Figure 1B). This was combined with a movement utility model to estimate planned movement time ((Shadmehr et al., 2016); Figure S6A and S5B) and a forward optimal controller to simulate reaching movements ((Todorov, 2005); Figure 1C and F, Figure S6C-D). Our simulation is briefly outlined below in steps.

Effective mass of the hand as a function of movement direction. We used a two-joint planar arm model to estimate the effective mass of the hand moving in different directions (Figure 1B). The parameters of the upper arm (length l_1, mass m_1, center of mass lc_1, inertia I_1) and the lower arm (length l_2, mass m_2, center of mass lc_2, inertia I_2) are based on values from Shadmehr et al., 2016:

$$l_1 = 0.33 \quad l_2 = 0.43 \qquad \text{m}$$

$$m_1 = 1.93 \quad m_2 = 1.52 \qquad \text{kg}$$

$$lc_1 = l_1/2 \quad lc_2 = 2l_2/3 \qquad \text{m}$$

$$I_1 = 0.014 \quad I_2 = 0.019 \qquad \text{kg.m}^2$$

The elbow and shoulder angles are denoted by θ_e and θ_s, respectively. The initial arm configuration is set by $\theta_s = 0.994$ rad, and $\theta_e = 1.5724$ rad, following the experimental conditions from Gordon et al., 1982. With a particular joint angle configuration, the end-point hand position is:

$$x = \left[l_1 \cos cos\, \theta_s + l_2 \cos cos \left(\theta_s + \theta_e\right);\ l_1 \sin sin\, \theta_s + l_2 \sin sin \left(\theta_s + \theta_e\right)\ \right]. \qquad \text{(eq.1)}$$

The arm's inertia matrix is:

$$I(\theta_s, \theta_e) = \left[I_{11},\ I_{12}; I_{21}, I_{22}\right], \qquad \text{(eq.2)}$$

where:

$$I_{11} = a_3 + a_1 l_1^2 + a_4 + 2a_2 l_1 cos\theta_e,\ I_{12} = I_{12} = a_2 + l_1 cos\theta_e + a_4,\ I_{22} = a_4,$$

with:

$$a_1 = m_2,\ a_2 = m_2 lc_2,\ a_3 = m_1 lc_1^2 + i_1,\ a_4 = m_2 lc_2^2 + i_2$$

The joint torques at the shoulder and elbow are represented as:

$$\tau = I(\theta)\ \ddot{\theta}, \qquad \text{(eq.3)}$$

and the forces at the hand are:

$$f = M(\theta)\ddot{x}\ . \qquad \text{(eq.4)}$$

We use the Jacobian matrix $\Lambda = \frac{dx}{d\theta}$ to relate force and torque, based on virtual work principle:

$$\tau = \Lambda^T f, \qquad \text{(eq.5)}$$

$$\dot{x} = \Lambda\dot{\theta}, \qquad \text{(eq.6)}$$

$$\ddot{x} = \dot{\Lambda}\dot{\theta} + \Lambda\ddot{\theta}. \qquad \text{(eq.7)}$$

Put S3 into S5:

$$f = \Lambda^{-1^T} I(\theta)\ \ddot{\theta}, \qquad \text{(eq.8)}$$

then combine S7 and S8:

$$f = \Lambda^{-1^T} I(\theta)\Lambda^{-1}\left(\ddot{x} - \dot{\Lambda}\dot{\theta}\right). \quad \text{(eq.9)}$$

Since the hand speed at the beginning of the movement is zero, according to S4 and S9, the mass matrix of hand $M(\theta)$ is:

$$M(\theta) = \Lambda^{-1^T} I(\theta)\Lambda^{-1}, \quad \text{(eq.10)}$$

The mass matrix $M(\theta)$ is a 2 x 2 matrix, and the effective mass $m(\theta)$ is determined by the length of the force vector when $M(\theta)$ is subjected to a unit acceleration.

In Figure S6A, the solid curve illustrates the effective mass across various directions under normal gravity, while the dashed curve represents the effective mass with a hypothetical 30% ($m_{0g}(\theta) = 0.3m(\theta)$)mass underestimation in microgravity. The colored lines indicate the effective mass amplitudes for the three target directions used in our experiment: 45°, 90°, and 135°.

Movement time determined by optimal utility. Following Shadmehr et al., 2016, the utility of an reaching action is given by:

$$J_{ut} = \frac{\alpha - amT - bmd^i/T^2}{1-\gamma T}, \quad \text{(eq.11)}$$

where α is the reward, m is mass, d is the distance to be moved, T is the planned duration of the movement, and a, b and i are scaling factors of the effort cost. γ represents a temporal discounting factor. The optimal movement time (T_{opt}) is the time that maximizes the utility J_{ut} :

$$T_{opt} = arg_T max\,(J_{ut}). \quad \text{(eq.12)}$$

The parameter values used in the simulation of Figure S6B were taken from Shadmehr 2016: $\alpha = 1000$, $a = 15$, $b = 100$, $i = 1.1$, $\gamma = 1$. The movement distance d is set as 0.12 m, the

target distance in the experiment. Figure S1B illustrates how the utility curves change with planned movement time in three experimental directions (45°, 90°, and 135°) under normal gravity, with colored dots indicating the optimal movement durations.

Movement kinematics simulated by optimal control theory. After setting the movement time T_{opt}, the position, speed and acceleration over time can be simulated based on an optimal control model (Todorov, 2005). The arm's control operates as a second-order low-pass filter:

$$u_t = \tau_1\tau_2\ddot{f}_t + \left(\tau_1 - \tau_2\right)\dot{f}_t + f_t, \qquad \text{(eq.13)}$$

with the time constants $\tau_1 = \tau_2 = 40ms$. The system state vector is $x = \left[p;\ \dot{p}; f; g; p^*\right]$, where p is position of hand, f is force acting on the hand, and g is an auxiliary state variable, p* is the target position. The control law is given by:

$$u_t = \tau_1\dot{g}_t + g_t,\ g_t = \tau_2\dot{f}_t + f_t.$$

The system dynamics are:

$$x_{t+1} = Ax_t + Bu_t,\ y_t = Hx_t, \qquad \text{(eq.14)}$$

$$A = \begin{bmatrix} 1 & dt & 0 & 0 & 0 \\ 0 & 1 & dt/m & 0 & 0 \\ 0 & 0 & 1 - dt/\tau_2 & dt/\tau_2 & 0 \\ 0 & 0 & 0 & 1 - dt/\tau_1 & 0 \\ 0 & 0 & 0 & 0 & 1 \end{bmatrix} \quad H = \begin{bmatrix} 1 & 0 & 0 & 0 & 0 \\ 0 & 1 & 0 & 0 & 0 \\ 0 & 0 & 1 & 0 & 0 \end{bmatrix}$$

$$B = \left[0; 0; 0; dt/\tau_1; 0\right].$$

The controller seeks to minimize the cost function J by optimizing the command u:

$$J = \int_0^\infty E\left[x^T Q x + u^T R u\right] dt. \qquad \text{(eq.15)}$$

For simulations in Figures 1C and 1F and Figures S5C and S5D, we used the penalty values from Todorov (2005) for each state and control variable: $w_u = 0.00001$, $w_p = 2$, $w_v = 0.2$, $w_f = 0.02$. The simulated speed and acceleration profiles are based on the optimal movement time T_{opt} from Figure S6B. From Figures S5C and S5D, we obtain the peak speed, peak acceleration, and their respective times.

In summary, we apply the movement utility theory to calculate the optimal movement time for a simplified two-joint arm moving in a 2D plane. This movement time is primarily determined by the effective mass and temporal discounting of reward. Next, we employ the optimal control theory to model the kinematics of hand movement, including its position, speed, and acceleration. This approach also enables us to estimate the peak speed and acceleration, as well as their respective times, for reaches performed toward different target directions. To simulate the effect of microgravity, we introduce a mass underestimation factor to account for the kinematic changes associated with this perceptual error.